AN ABSTRACT OF THE THESIS OF

Bert Lee Barnes for the degree of Civil Engineer in Civil Engineering

presented on May 12, 1975

Title: Experiments on Cable Strumming and Flow Induced Drag

Abstract approved: Redacted for Privacy

Dr. L. S. Slotta

Short non-flexible elements of cable were driven harmonically in water while constrained by springs. The cable elements were observed to oscillate at approximately the Strouhal vortex shedding frequency. Damped resonance occurred near the point where the natural frequency and the Strouhal vortex shedding frequency were equal. Transverse oscillation amplitudes greater than one and one half cable diameters and hydrodynamic drag forces as much as seven times that normally experienced by rigidly constrained cylinders were observed in the neighborhood of the resonance point. A simple second order mathematical model was constructed which closely approximates the cable elements transverse response in the neighborhood of the resonance point.

EXPERIMENTS ON CABLE STRUMMING

AND

FLOW INDUCED DRAG

by

Bert Lee Barnes

A THESIS

submitted to

Oregon State University

in partial fulfillment of
the requirements for the
degree of

Civil Engineer

Completed May 12, 1975

Commencement June 1975

APPROVED:

Redacted for Privacy

Professor of Civil Engineering

Redacted for Privacy

Head of Department Civil Engineering

Redacted for Privacy

Dean of Graduate School

Date thesis is presented May 12, 1975

Typed by Louise Auchampach for Bert Lee Barnes

AKNOWLEDGMENT

This research was supported by the National Oceanic and Atmospheric Administration (maintained by U.S. Department of Commerce) Institutional Sea Grant Contract 2-35187, at Oregon State University.

TABLE OF CONTENTS

I. Introduction 1

II. Apparatus 7

III. Procedure 10

IV. Results 13

V. Approximate Linear Equivalent System 51

VI. Conclusions 55

VII. Bibliography 57

IX. List of Nomenclature 59

LIST OF ILLUSTRATIONS

Figure		Page
1.	Karman Vortex Street in the Wake of A Cylinder	2
2.	Schematic Diagram of Experimental Apparatus	8
3.	Pluck Test From Run #8 Oscillograph Trace	11
4.	Peak-to-Peak Oscillation Amplitude, Run #5	20
5.	Peak-to-Peak Oscillation Amplitude, Run #8	21
6.	Peak-to-Peak Oscillation Amplitude, Run #20-5.4	22
7.	Peak-to-Peak Oscillation Amplitude, Run #20-10.5	23
8.	Peak-to-Peak Oscillation Amplitude, Run #20-20.5	24
9.	Summary of Peak-to-Peak Oscillation Amplitude Data	25
10.	Common Linear Second Order Response Curve	26
11.	Common Linear Second Order Amplitude Ratio Curve	26
12.	Peak Response Amplitude and Stroke Length	28
13.	Trace of Typical Oscillograph Plot	30
14.	Drag Envelope, Run #5	32
15.	Drag Envelope, Run #8	33
16.	Drag Envelope, Run #20-5.4	34
17.	Drag Envelope, Run #20-10.5	35
18.	Drag Envelope, Run #20-20.5	36
19.	Summary of Drag Envelope Plots	37
20.	Frequency Variation, Run #5	39
21.	Frequency Variation, Run #8	40
22.	Frequency Variation, Run #20-5.4	41

LIST OF ILLUSTRATIONS CONT.

Figure		Page
23.	Frequency Variation, Run #20-10.5	42
24.	Frequency Variation, Run #20-20.5	43
25.	Actual Oscillation Frequency and Expected Exciting Frequency, Run #5	44
26.	Actual Oscillation Frequency and Expected Exciting Frequency, Run #8	45
27.	Actual Oscillation Frequency and Expected Exciting Frequency, Run #20-5.4	46
28.	Actual Oscillation Frequency and Expected Exciting Frequency, Run #20-10.5	47
29.	Actual Oscillation Frequency and Expected Exciting Frequency, Run #20-20.5	48
30.	Summary Plot of Actual Oscillation Frequency and Expected Exciting Frequency	49

EXPERIMENTS ON CABLE STRUMMING AND FLOW INDUCED DRAG

INTRODUCTION

With an ever increasing level of human activity in the oceans, mooring problems are of necessity receiving much more attention and thought. One such problem deals with the hydrodynamic drag on a cable which is either moving through quiescent water or is stationary and subjected to water movement caused by some combination of tidal currents, wind, and waves.

For any relative motion of a cable in water above a Reynolds Number of 50, vortices are formed near the downstream boundaries of the cable/water interface and are shed in a predictable uniform manner. This shedding of vortices was first investigated by T. von Karman in 1911. Figure 1 is typical of what is commonly called a Karman vortex street. The vortices are shed from alternate sides and have opposite rotational directions. The number of vortex pairs flowing off per second are given by the expression:

$$f_s = S\dot{X}/D, \ sec^{-1} \qquad (1)$$

where S is the Strouhal Number (generally around 0.20), $\dot{X}$ is the relative velocity of the fluid stream (ft/sec), and D is the cable diameter (ft). This equation is normally defined only for steady flow ($\dot{X}$ = constant). However, preliminary analysis of experimental results have shown that the equation is reasonably accurate for moderately varying unsteady flow as well and its use facilitates comparison with similar steady state experiments. Examining this phenomenon in more detail, the observer finds that these vortices are unstable elements in the downstream cylinder/fluid interface which are shed from the cylinder

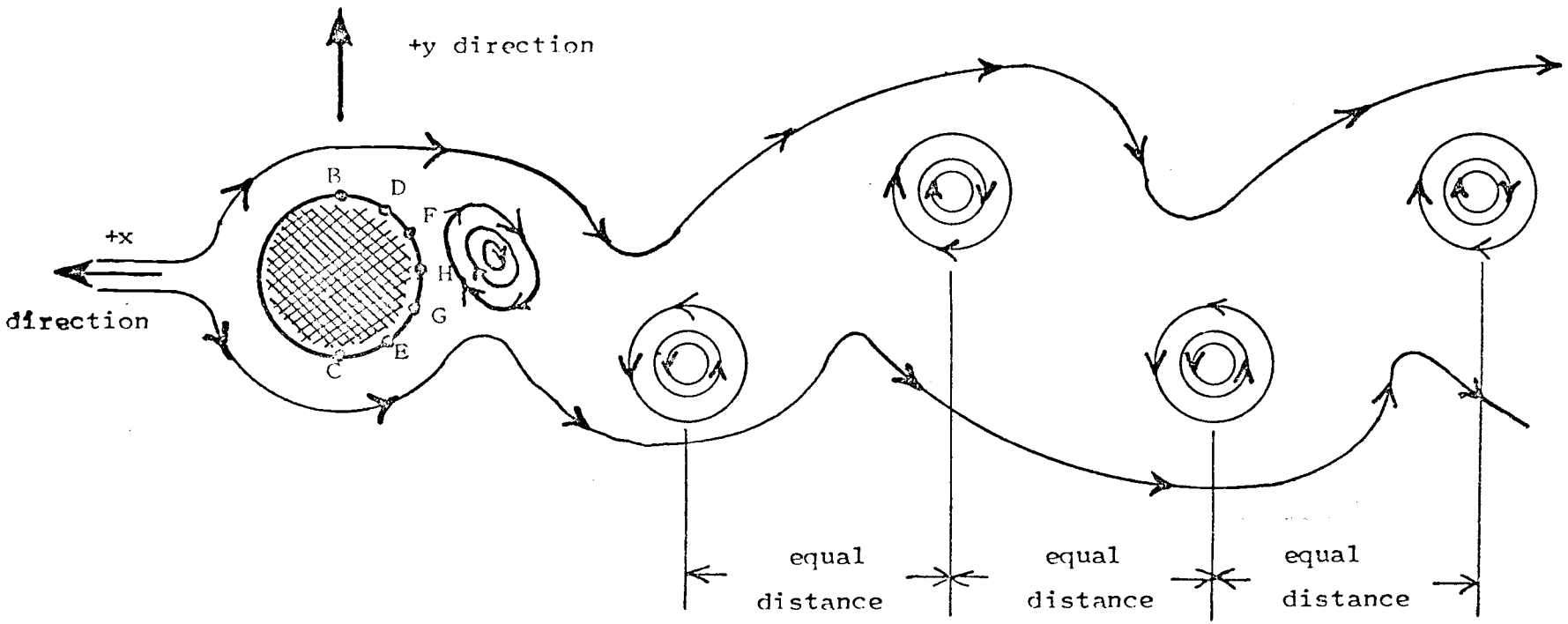

FIGURE 1. Karman vortex street in the wake of a cylinder.

by some combination of the effects of the location of the vortex in the adverse pressure gradient of the cylinder, and viscous, inertial and pressure forces. In a cylinder moving through quiesant fluid in a single direction, vortices are formed in the adverse pressure gradient near the downstream most portions of the cylinder (Figure 1, HF and HG). These vortices then move forward along the cylinder/fluid interface within and under the influence of the adverse pressure gradient (from area HF and HG) until they approach points D or E, where they are cast off into the wake.

As a result of these vortices being shed alternately from either side of the cable, there is at any one instant an imbalance of pressure forces acting on the cable. The vectorial resultant of these imbalanced pressure forces is a more or less harmonically varying force having components both perpendicular and parallel to the direction of the current. For a flexibly constrained cylinder, such as a taut cable, this force unbalance produces oscillations which are both perpendicular and parallel to the direction of flow, the oscillations in the y direction (perpendicular) being in general larger than the oscillations in the x direction (parallel).

The author speculates that the frequency at which vortices are shed from an oscillating cylinder, as described above, may be significantly different than from a similar rigidly constrained cylinder. There are two good reasons that this should be true.

First, an oscillating cylinder has a larger mean velocity, since its velocity is the instantaneous vector sum of all forward ($\dot{X}$) and all lateral ($\dot{Y}$) components of velocity. If the parameter $\dot{x}$ in

equation (1) is replaced with this vector sum of velocities, one can see that an increase in the Strouhal frequency will result since the frequency is proportional to velocity.

Secondly, vortices are known to be signs of instabilities within the adverse pressure gradient which are shed as some function of the position of the vortex along the adverse pressure gradient and the combined effects of viscous, inertial and pressure forces acting on the vortex. The adverse pressure gradient for an oscillating cylinder should be subject to more movement around the perimeter of the cylinder than would the adverse pressure gradient for a similar stationary cyli cylinder. A given vortex can, as a result of this motion, reach the geometric position where it would normally be shed either sooner or later than it would for a similar non-oscillating cylinder. Also, the inertial forces which act on the vortex are greater for an oscillating cylinder than for a non-oscillating cylinder. The large inertial forces accompanying the continuous changes in velocity and direction should also tend to "throw off" vortices at a faster rate than the Strouhal equation [1] would predict.

The flow induced oscillations described above are commonly observed not only in taut cables but in electrical wires strung between phone poles acted upon by the wind, submarine periscopes, bridge pilings, heat exchanger tubes, tall chimneys or any other place where a fluid moves past a cylindrical or bluff cross section which is elastically constrained. Though these experiments were directed toward flow induced oscillations on mooring cables, commonly called cable "strumming", the results may be applied to other similar problems

whose spring-mass and fluid parameters fall within the bounds of those parameters considered here.

Strumming cables have been observed to exhibit abnormally high values of hydrodynamic drag which result in a periodic variation in cable tension. Such variations in tension could easily result in cable failure by some combination of internal abrasion and by exceeding the cyclic endurance limit of the cable.

The strumming effect is maximized at resonance, when the exciting frequency (approximately equal to the Strouhal vortex shedding frequency) equals the natural frequency of the cable. Since a cable has an infinite number of natural frequencies above its first mode natural frequency, significant strumming could be expected any time the exciting frequency exceeds the first mode natural frequency of the cable. Omitting considerations of damping for the moment and considering only small amplitude vibrations, the first mode natural frequency of a taut cable is given by the solution of the one dimensional wave equation as

$$f_c = \frac{(Tg/w)^{\frac{1}{2}}}{2\ell} \quad , \text{ cycles per second} \qquad (2)$$

where ℓ is the length of the cable (ft), T is the tension (lbs), g the acceleration of gravity, and w is the weight per foot (lbs/ft) of the cable. The effect of damping is to reduce this frequency. The results of this study showed that the reduction in frequency due to the damping was between eight and fifteen percent for the particular parameters considered here. These specific parameters also gave oscillations up to one and one half cable diameters peak-to-peak at and near resonance.

In this series of experiments, a simple harmonic driving motion was used and the induced oscillations perpendicular (transverse) to this applied motion were observed. A simple harmonic motion was used for the following reasons:

a) Previous experiments by Laird (9 & 10) showed curious results using harmonic motion in similar experiments. Experiments by Bidde (2) and Keulegan and Carpenter (8) also indicated that there was much to learn by this method though they themselves did not follow this exact procedure.

b) Some types of mooring problems, such as buoys anchored in shallow water subjected to wave action, are subject to motions well modeled by simple harmonic motion.

c) The facilities available to the author particularly lended themselves to experiments of this type.

It was the intent of this study to determine the magnitude of the cable oscillations and the maximum drag when the cable natural frequency was approached by the Strouhal exciting frequency. The Strouhal frequency was defined arbitrarily at the maximum impressed harmonic velocity ($\dot{X}_{max}$).

APPARATUS

Figure 2 illustrates the experimental apparatus used for this series of experiments. Elements of cable (A) with wetted lengths of 18.25 to 19.5 inches were harmonically driven in the X direction at various selected speeds. The cable element was attached to a light-weight cross-carriage with small roller bearings for wheels (D). The small roller bearing wheels ran in smooth extruded aluminum tracks (C). Element (B) served the dual purpose of connecting the cable element (A) to the cross-carriage (D) and also held two strain gage bridges for measuring the X and Y components of force applied to the cable element. The cross-carriage was constrained from moving in the Y direction by means of two linear coil springs (E). In series with one of these coil springs was a small strain gage transducer (F) which measured the amplitude of the carriage motion in the Y direction. There was also an engineering scale and movable pointer attached to the track and cross-carriage which was used for static calibration of the Y displacement transducer. The main carriage (G) was harmonically driven back and forth in the X direction on two smooth greased stationary rails (M) by means of a connecting rod (H), a variable radius crank wheel (I), and a variable speed drive motor (L). The X displacement was measured by an eccentric round wheel (J) and an X displacement strain gage transducer (K).

Output signals from the four strain gage transducers measuring forces and displacements in the X and Y directions were fed into four separate amplifiers which in turn were fed into a four channel

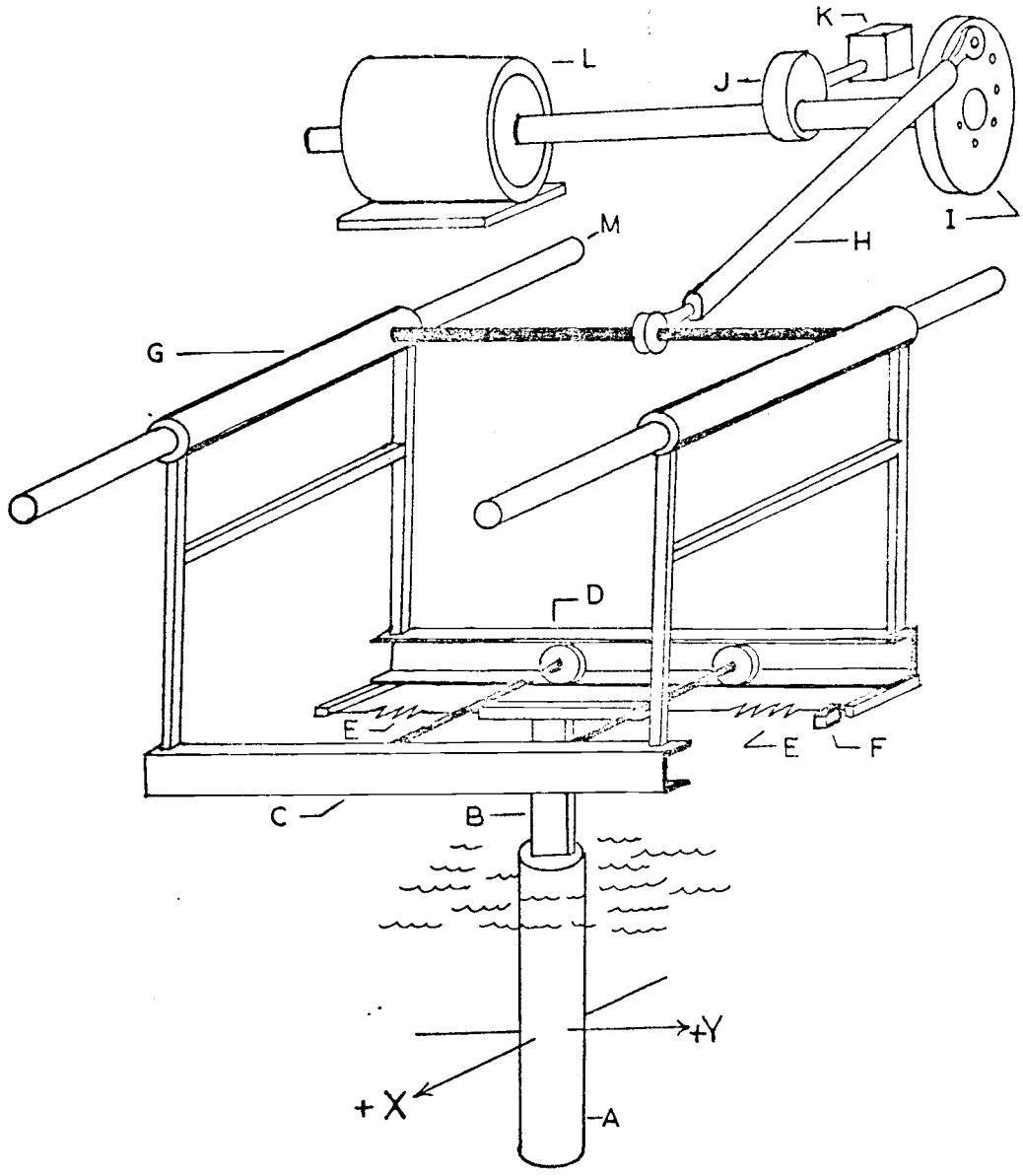

FIGURE 2.

Schematic diagram of experimental apparatus.

oscillograph employing light beams and photo sensitive recording paper. This enabled the resulting instantaneous values of force and displacement to be compared by reading in a vertical line up and down the oscillograph chart. Only the average X displacement (main carriage movement) was measured; no provision was made for measuring the instantaneous X displacement superimposed upon the main carriage by the amount of the relative motion across the flexible connecting member (B) as shown in Figure 2.

The entire experiment was run in a shallow wave basin filled with water to an approximate depth of twenty inches. A large stationary shim was placed under the end of the cable elements and adjusted such that the clearance between the bottom end of the cable element and the shim was 0.060 inch. The purpose of this shim was to minimize end effects (maximize the aspect ratio) by minimizing flow about the end of the cable element.

Both the 1-3/4 inch diameter cable element and the 1-1/8 inch diameter cable element were made from lightweight aluminum tube with sealed ends. Weight was added to the cross-carriage to make the total weight, including the cable element, closely approximate the weight of steel cable.

PROCEDURE

Calibrations of both X and Y force and Y displacement transducers were made before and after each run using a set of static calibration weights and an engineer's scale. A fine wire was passed over a series of low friction pulleys in such a way that a calibration weight hung on one end of the wire produced a normal force equal to its weight at the center of the wetted length of the cable element. By hanging various weights on the end of the wire, the X and Y forces were related to the deflection shown on the oscillograph chart. An engineer's scale was used to relate deflection of the cross-carriage with the Y displacement reading on the oscillograph.

In addition to the calibrations, a "pluck test" was performed by physically displacing the cross-carriage in the Y direction and releasing it. One such typical Y displacement curve generated on the oscillograph is shown in Figure 3. By counting the number of observed cycles and measuring the time on the oscillograph chart, the damped natural frequency f_{ny} was obtained for each run. Since the system was known to be nonlinear, such that the natural frequency of the cable was to some minor extent a function of the amplitude of the oscillation, care was taken to calculate f_{ny} at amplitudes bracketing the observed maximum amplitudes at resonance in order to minimize the effects of nonlinearity in the vicinity of the point of resonance.

A run consisted of operating the drive motor, Figure 2, at various constant speeds such that the cable element was moved through four to five cycles in the X direction at each speed before moving on to the

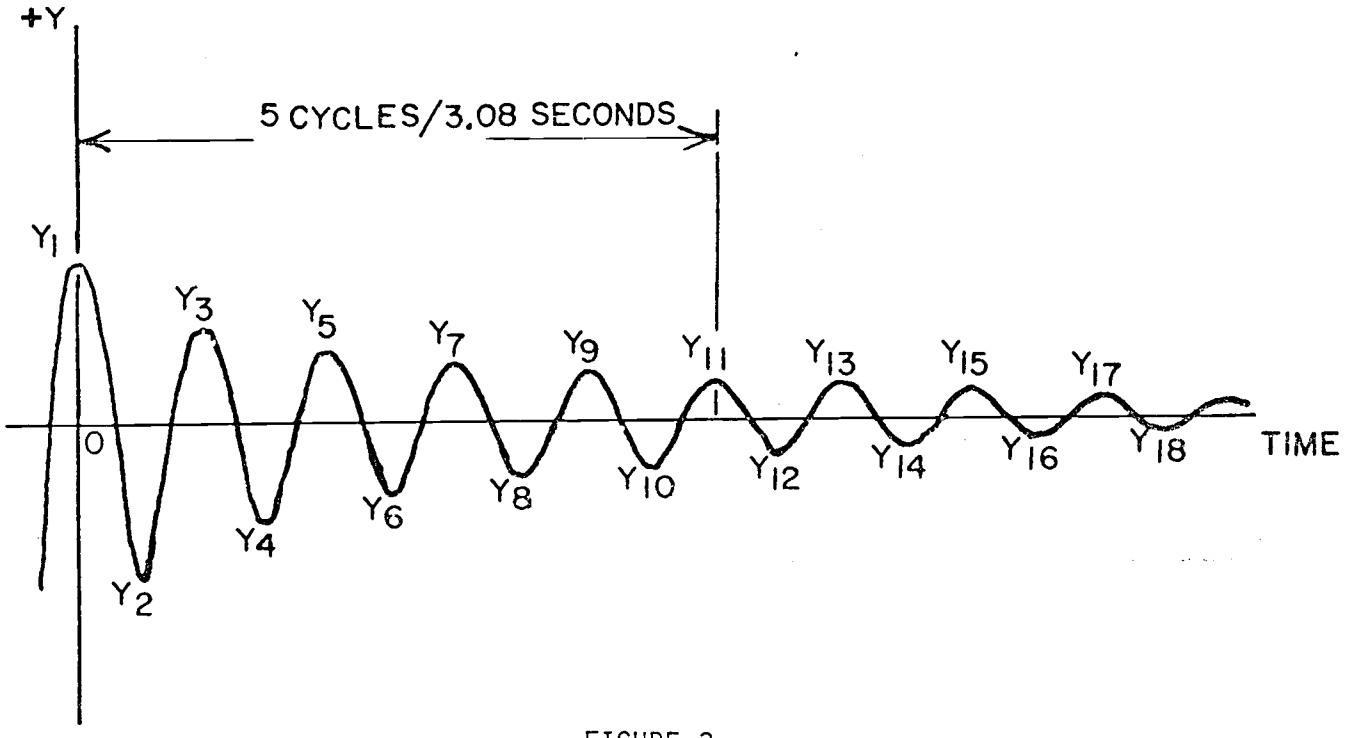

FIGURE 3.

Pluck test from run #8 oscillograph trace.

next speed. The results were observed to become repetative after the first or second cycle so it was only necessary to record four or five cycles to assure good results. The number of different speeds was determined in each case by two criteria. The lower speed limit was determined by watching the amplitude of the Y oscillation until it had decreased to a value beyond which the Y displacement transducer gave an insignificant output. The upper speed limit was generally limited by the capabilities of the transducers; to go to any higher speed would have damaged the transducers.

Since the force measuring transducers actually measured both hydrodynamic forces and inertial forces on the cable element, a simple experiment was performed to determine the relative magnitudes of the two force signals. The entire apparatus including the cable element was operated in the absence of water at the upper limits of amplitude and frequency thus maximizing the acceleration and hence the inertial force in the X direction. The resulting inertial force signals were very small in comparison to the hydrodynamic drag forces that were measured under the same conditions when the tank was full of water.

RESULTS

All data were analyzed and put in tabular and graphical form. All listed frequencies, forces, and displacements obtained from this series of experiments have been averaged. Tables I, II, III, IV, V and VI summarize this graphical data for the various cable sizes and weights considered.

Note that Table I lists a considerable range in weight per foot for real steel cables. The reason for this wide variation in cable weights results from the various methods of cable construction, different core materials, and intended applications. The weight per foot of the models used in these tests does, with one exception, fall within the range of listed weights for both sizes of steel cables.

The tabular data in Tables II, III, IV, V, and VI have been arranged in a consistent format to facilitate comparison of the various runs.

Figures 4, 5, 6, 7 and 8 show for each case the peak-to-peak oscillation amplitudes in the neighborhood of system damped resonance. Figure 9 is a similar plot showing the curves of Figures 4, 5, 6, 7 and 8 superimposed upon one another. The basic shapes of the curves are in each case reasonably close to what might be expected of a common linear second order spring-mass system, the peak values of amplitude being where the damped natural frequency is approximately equal to the Strouhal vortex shedding frequency.

Figures 10 and 11 have been included to aid the reader in comparing the non-linear responses shown in Figure 9 with that of a linear

TABLE I. REAL AND MODELED CABLE PARAMETERS

Run Number	Stroke, A (inches)	Cable Diameter, D (inches)	Wetted Length of Cable D, l (inches)	Equivalent Cable Mass, M (Slugs)	Equivalent Cable Weight per Wetted Foot (lb/ft)	Weight Range per Foot of Real Steel Cable D inches in Diameter Ref. 11 (lb/ft)
5	20.5	1.750	19.5	0.120	2.38	3.22 to 6.59
8	20.5	1.750	19.5	0.244	4.83	3.22 to 6.59
20	5.4	1.125	18.25	0.119	2.52	1.33 to 2.70
20	10.5	1.125	18.25	0.119	2.57	1.33 to 2.70
20	20.5	1.125	18.25	0.119	2.52	1.33 to 2.70

TABLE II. TABULAR DATA FROM RUN #5.

Cable Size: 1-3/4" diameter
Cable Element Length: 19.5" wetted
Constraining Springs: 30.0 lb/ft in Y direction
Undamped Natural Frequency = $\omega_N = (K/m)^{1/2}$ = 2.52 cps

Mass = m = 0.120 slugs
Natural Frequency Damped, Pluck Test: f_{ny} = 2.25 cps
Water Temperature: 68 degrees, F
Calculated Damping Ratio = $r = (1-(f_{ny}/\omega_N)^2)^{1/2}$ = 0.450

Driven Frequency f_d, cps	Driven Amplitude A, inches	Frequency Ratio f_{ny}/f_s	Strouhal Frequency $f_s = S\dot{X}_{max}D^{-1}$, cps S*=0.165	Velocity Driven $\dot{X}_{max}$, ft/sec	Transverse Displacement, Y_{max}, inches	Frequency f_y, cps	Drag Force F_{xmax} lb	Drag Force F_{xmin} lb	Reynolds Number = $\dot{X}_{max}D/\nu \times 10^{-4}$	Calculated Drag Force*, F, lb, and Coefficient C_d
0.308	20.5	0.601	3.74	3.31	1.06	2.45	4.47	2.48	4.46	3.00 / 1.20
0.296	20.5	0.625	3.60	3.18	1.11	2.38	3.98	2.20	4.28	2.78 / 1.20
0.274	20.5	0.678	3.32	2.94	1.12	2.31	3.85	2.05	3.96	2.38 / 1.20
0.245	20.5	0.759	2.97	2.63	1.31	2.33	4.00	1.60	3.54	1.90 / 1.20
0.222	20.5	0.825	2.73	2.41	1.35	2.29	3.44	1.54	3.24	1.60 / 1.20
0.185	20.5	1.000	2.25	1.99	1.44	2.09	3.34	1.18	2.68	1.09 / 1.20
0.170	20.5	1.085	2.07	1.83	1.45	1.94	2.97	0.82	2.46	0.92 / 1.20
0.156	20.5	1.190	1.89	1.67	1.45	1.99	2.94	0.85	2.25	0.77 / 1.20
0.142	20.5	1.305	1.723	1.52	1.35	1.95	2.53	0.79	2.05	0.64 / 1.20
0.129	20.5	1.440	1.565	1.39	1.30	1.93	2.20	0.41	1.86	0.53 / 1.20

* The value of S was selected from Reference (1) as being representative of S over the range of Reynolds Numbers between 10^3 and 10^5. The Strouhal Number S is fairly constant over this range of Reynolds Numbers for circular cylinders. F, the calculated drag force, is based upon the equation $F = \frac{1}{2}C_d\rho A(\dot{X}_{max})^2$ where Cd has been selected from Reference (1) using the value of Reynolds Number shown.

TABLE III. TABULAR DATA FROM RUN #8.

Cable Size: 1-3/4" diameter
Cable Element Length: 19.5" wetted
Constraining Springs: 30.0 lb/ft in Y direction
Undamped Natural Frequency $= \omega_N = (K/m)^{1/2} = 1.76$ cps

Mass = m = 0.244 slugs
Natural Frequency Damped, Pluck Test: $f_{ny} = 1.62$ cps
Water Temperature: 68 degrees, F
Calculated Damping Ratio = $r = (1-(f_{ny}/\omega_N)^2)^{1/2} = 0.392$

Driven Frequency f_d, cps	Driven Amplitude A, inches	Frequency Ratio f_{ny}/f_s	Strouhal Frequency $f_s = S\dot{X}_{max}D^{-1}$, cps S*=0.165	Velocity Driven $\dot{X}_{max}$, ft/sec	Transverse Displacement, Y_{max}, inches	Frequency f_v, cps	Drag Force F_{xmax} lb	Drag Force F_{xmin} lb	Reynolds Number = $\dot{X}_{max}D/\nu \times 10^{-4}$	Calculated Drag Force*, F, lb, and Coefficient C_d
0.308	20.5	0.434	3.74	3.31	0.35	1.93	4.21	2.13	4.46	3.00 / 1.20
0.290	20.5	0.459	3.53	3.12	0.55	1.98	3.84	1.75	4.20	2.68 / 1.20
0.260	20.5	0.511	3.17	2.80	0.74	1.92	3.58	1.25	3.77	2.16 / 1.20
0.235	20.5	0.566	2.86	2.53	0.80	1.80	2.59	1.05	3.41	1.76 / 1.20
0.213	20.5	0.625	2.59	2.29	0.76	1.77	2.16	0.956	3.08	1.44 / 1.20
0.197	20.5	0.675	2.40	2.12	0.86	1.80	2.21	0.994	2.86	1.24 / 1.20
0.185	20.5	0.814	2.25	1.99	1.00	1.77	2.03	0.755	2.68	1.09 / 1.20
0.149	20.5	0.895	1.81	1.60	1.10	1.76	1.49	0.561	2.15	.705/ 1.20
0.154	20.5	0.855	1.875	1.66	1.23	1.87	1.84	0.700	2.23	.755/ 1.20
0.137	20.5	0.970	1.67	1.48	1.35	1.65	1.39	0.565	1.99	.597/ 1.20
0.125	20.5	1.065	1.52	1.34	1.33	1.63	1.16	0.408	1.81	.497/ 1.20
0.117	20.5	1.132	1.43	1.27	1.28	1.56	1.20	0.394	1.72	.440/ 1.20
0.103	20.5	1.290	1.26	1.11	0.70	1.57	0.950	0.208	1.49	.336/ 1.15
0.0804	20.5	1.660	0.976	0.864	0.20	1.25	0.566	-0.27	1.16	.204/ 1.15
0.0856	20.5	1.540	1.05	0.931	0.390	1.45	0.774	-0.105	1.25	.237/ 1.15
0.1125	20.5	1.18	1.37	1.21	1.06	1.56			1.63	.403/ 1.15
0.0796	20.5	1.675	0.966	0.855	0.250	1.25	0.575	-0.150	1.15	.199/ 1.15
0.0688	20.5	1.94	0.835	0.739	0.090	1.05	0.322	-0.065	0.99	.125/ 1.00

* The value of S was selected from Reference (1) as being representative of S over the range of Reynolds Numbers between 10^3 and 10^5. The Strouhal Number S is fairly constant over this range of Reynolds Numbers for circular cylinders. F, the calculated drag force, is based upon the equation $F = \frac{1}{2}C_d\rho A(\dot{X}_{max})^2$ where Cd has been selected from Reference (1) using the value of Reynolds Number shown.

TABLE IV. TABULAR DATA FROM RUN #20-5.4.

Cable Size: 1-1/8" diameter
Cable Element Length: 18.25" wetted
Constraining Springs: 16.8 lb/ft in Y direction
Undamped Natural Frequency = $\omega_N = (K/m)^{1/2} = 1.89$ cps

Mass = m = 0.119 slugs
Natural Frequency Damped, Pluck Test: $f_{ny} = 1.61$ cps
Water Temperature: 68 degrees, F
Calculated Damping Ratio = $r = (1-(f_{ny}/\omega_N)^2)^{1/2} = 0.524$

Driven Frequency f_d, cps	Driven Amplitude A, inches	Frequency Ratio f_{ny}/f_s	Strouhal Frequency $f_s = S\dot{X}_{max}D^{-1}$, cps S*=0.16	Velocity Driven $\dot{X}_{max}$, ft/sec	Transverse Displacement, Y_{max}, inches	Frequency f_y, cps	Drag Force F_{xmax} lb	Drag Force F_{xmin} lb	Reynolds Number = $\dot{X}_{max}D/\nu \times 10^{-3}$	Calculated Drag Force*, F, lb, and Coefficient C_d
0.739	5.40	0.436	3.69	2.09	0.18	2.21	0.870	0.761	17.03	0.741 /1.23
0.711	5.40	0.441	3.65	2.01	0.18	2.19	0.826	0.635	16.38	0.680 /1.22
0.655	5.40	0.479	3.36	1.85	0.18	2.37	0.692	0.530	15.10	0.574 /1.21
0.583	5.40	0.536	3.00	1.65	0.27	2.17	0.593	0.415	13.44	0.442 /1.17
0.508	5.40	0.617	2.61	1.44	0.62	2.00	0.509	0.304	11.72	0.328 /1.15
0.326	5.40	0.964	1.67	0.923	0.68	1.64	0.407	0.115	7.52	0.125 /1.05
0.292	5.40	1.075	1.50	0.826	0.43	1.64	0.231	0.061	6.73	0.0979/1.04
0.253	5.40	1.240	1.30	0.715	0.29	1.55	0.215	0.018	5.82	0.0701/.994
0.224	5.40	1.40	1.15	0.633	0.19	1.59	0.185	0.0037	5.15	0.0541/.973
0.191	5.40	1.64	0.98	0.540	0.14	1.31	0.140	-0.015	4.40	0.0386/.953
0.168	5.40	1.87	0.86	0.475	0.03	1.16	0.090	-0.0059	3.87	0.0296/.950

* The value of S was selected from Reference (1) as being representative of S over the range of Reynolds Numbers between 10^3 and 10^5. The Strouhal Number S is fairly constant over this range of Reynolds Numbers for circular cylinders. F, the calculated drag force, is based upon the equation $F = \frac{1}{2}C_d\rho A(\dot{X}_{max})^2$ where Cd has been selected from Reference (1) using the value of Reynolds Number shown.

TABLE V. TABULAR DATA FROM RUN #20-10.5.

Cable Size: 1-1/8" diameter
Cable Element Length: 18.25" wetted
Constraining Springs: 16.8 lb/ft in Y direction
Undamped Natural Frequency $= \omega_N = (K/m)^{1/2} = 1.89$ cps

Mass = m = 0.119 slugs
Natural Frequency Damped, Pluck Test: $f_{nv} = 1.61$ cps
Water Temperature: 63 degrees, F
Calculated Damping Ratio = $r = (1-(f_{nv}/\omega_N)^2)^{1/2} = 0.524$

Driven Frequency f_d, cps	Driven Amplitude A, inches	Frequency Ratio f_{ny}/f_s	Strouhal Frequency $f_s = S\dot{X}_{max}D^{-1}$, cps S*=0.16	Velocity Driven $\dot{X}_{max}$, ft/sec	Transverse Displacement, Y_{max}, inches	Frequency f_y, cps	Drag Force F_{xmax} lb	Drag Force F_{xmin} lb	Reynolds Number = $\dot{X}_{max}D/\nu \times 10^{-3}$	Calculated Drag Force*, F, lb, and Coefficient C_d
0.326	10.5	0.494	3.26	1.80	0.390	1.86	0.705	0.500	14.65	0.534 / 1.20
0.314	10.5	0.512	3.14	1.73	0.420	1.85	0.715	0.465	14.10	0.491 / 1.19
0.292	10.5	0.552	2.92	1.61	0.480	1.81	0.712	0.435	13.10	0.420 / 1.17
0.291	10.5	0.554	2.91	1.60	0.500	1.90	0.798	0.449	13.05	0.410 / 1.17
0.270	10.5	0.596	2.70	1.48	0.505	1.94	0.600	0.326	12.10	0.353 / 1.15
0.248	10.5	0.648	2.48	1.36	0.505	1.85	0.493	0.255	11.10	0.294 / 1.14
0.222	10.5	0.725	2.22	1.22	0.510	1.82	0.596	0.129	9.95	0.232 / 1.13
0.193	10.5	0.834	1.93	1.06	0.515	1.76	0.565	-0.034	8.65	0.171 / 1.11
0.161	10.5	1.003	1.61	0.885	0.520	1.67	0.343	0.010	7.22	0.113 / 1.04
0.102	10.5	1.58	1.02	0.561	0.045	1.61	0.300	-0.136	4.57	0.0419/ .965
0.0839	10.5	1.80	0.896	0.494	0.030	1.37	0.125	-0.08	4.03	0.0320/ .950
0.0752	10.5	2.15	0.750	0.413	0.010	1.16	0.102	-0.063	3.37	0.0223/ .950

* The value of S was selected from Reference (1) as being representative of S over the range of Reynolds Numbers between 10^3 and 10^5. The Strouhal Number S is fairly constant over this range of Reynolds Numbers for circular cylinders. F, the calculated drag force, is based upon the equation $F = \frac{1}{2}CdpA(\dot{X}_{max})^2$ where Cd has been selected from Reference (1) using the value of Reynolds Number shown.

TABLE VI. TABULAR DATA FROM RUN #20.20.5.

Cable Size: 1-1/8" diameter
Cable Element Length: 18.25" wetted
Constraining Springs: 16.8 lb/ft in Y direction
Undamped Natural Frequency $= \omega_N = (K/m)^{1/2} = 1.89$ cps

Mass = m = 0.119 slugs
Natural Frequency Damped, Pluck Test: $f_{ny} = 1.61$ cps
Water Temperature: 68 degrees, F
Calculated Damping Ratio = $r = (1-(f_{nv}/\omega_N)^2)^{1/2} = 0.524$

Driven Frequency f_d, cps	Driven Amplitude A, inches	Frequency Ratio f_{ny}/f_s	Strouhal Frequency $f_s = S\dot{X}_{max}D^{-1}$, cps S*=0.16	Velocity Driven $\dot{X}_{max}$, ft/sec	Transverse Displacement, Y_{max}, inches	Frequency f_y, cps	Drag Force F_{xmax} lb	Drag Force F_{xmin} lb	Reynolds Number = $\dot{X}_{max}D/\nu \times 10^{-3}$	Calculated Drag Force*, F, lb, and Coefficient C_d
0.1015	20.5	0.812	1.98	1.090	0.380	1.92	0.425	0.072	8.89	0.181 / 1.10
0.100	20.5	0.826	1.95	1.075	0.365	1.93	0.455	0.077	8.75	0.175 / 1.10
0.099	20.5	0.835	1.93	1.065	0.300	1.85	0.397	0.032	8.67	0.171 / 1.09
0.0935	20.5	0.883	1.83	1.007	0.400	1.88	0.432	-0.058	8.20	0.150 / 1.07
0.0825	20.5	1.002	1.60	0.885	0.438	1.74	0.429	-0.090	7.22	0.113 / 1.05
0.0775	20.5	1.065	1.51	0.833	0.230	1.60	0.350	-0.090	6.79	0.098 / 1.03
0.0705	20.5	1.175	1.37	0.756	0.160	1.55	0.337	-0.233	6.16	0.079 / 1.00
0.0518	20.5	1.60	1.01	0.556	0.030	1.31	0.291	-0.192	4.54	0.043 / .995

* The value of S was selected from Reference (1) as being representative of S over the range of Reynolds Numbers between 10^3 and 10^5. The Strouhal Number S is fairly constant over this range of Reynolds Numbers for circular cylinders. F, the calculated drag force, is based upon the equation $F = \frac{1}{2}C_d\rho A(\dot{X}_{max})^2$ where Cd has been selected from Reference (1) using the value of Reynolds Number shown.

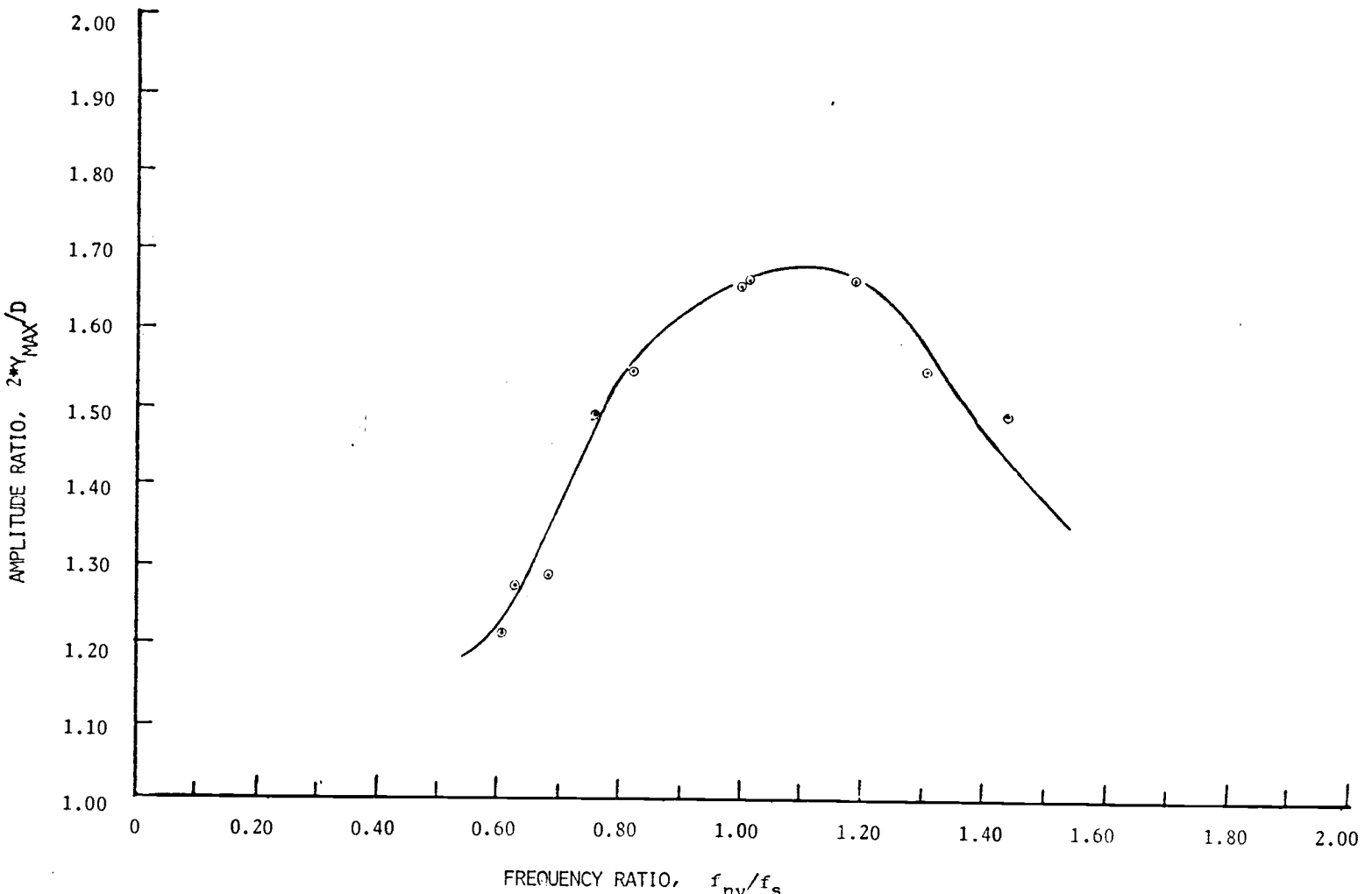

FIGURE 4. Peak-to-peak oscillation amplitude, run #5.

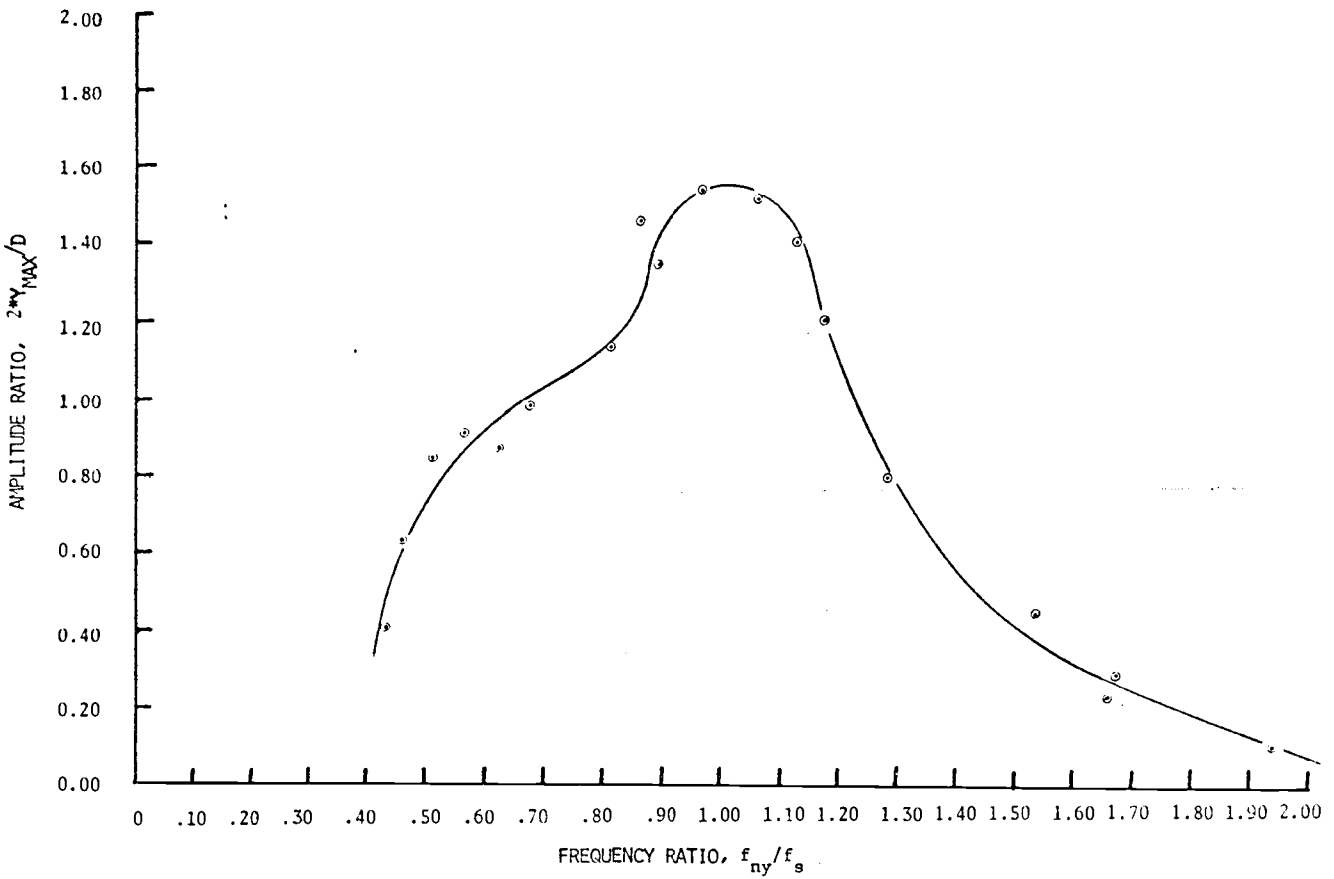

FIGURE 5. Peak-to-peak oscillation amplitude, run #8.

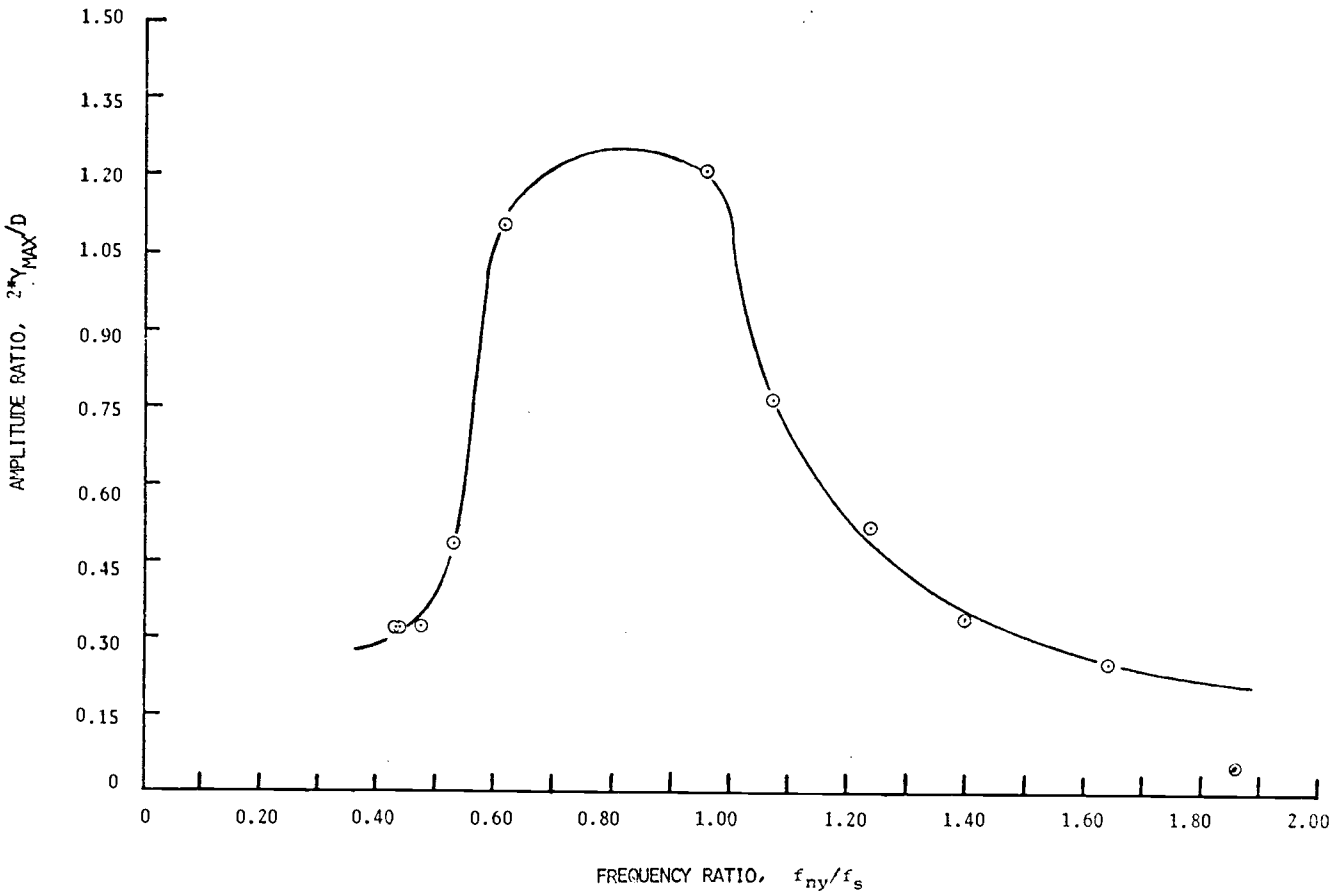

FIGURE 6. Peak-to-peak oscillation amplitude, run #20-5.4 .

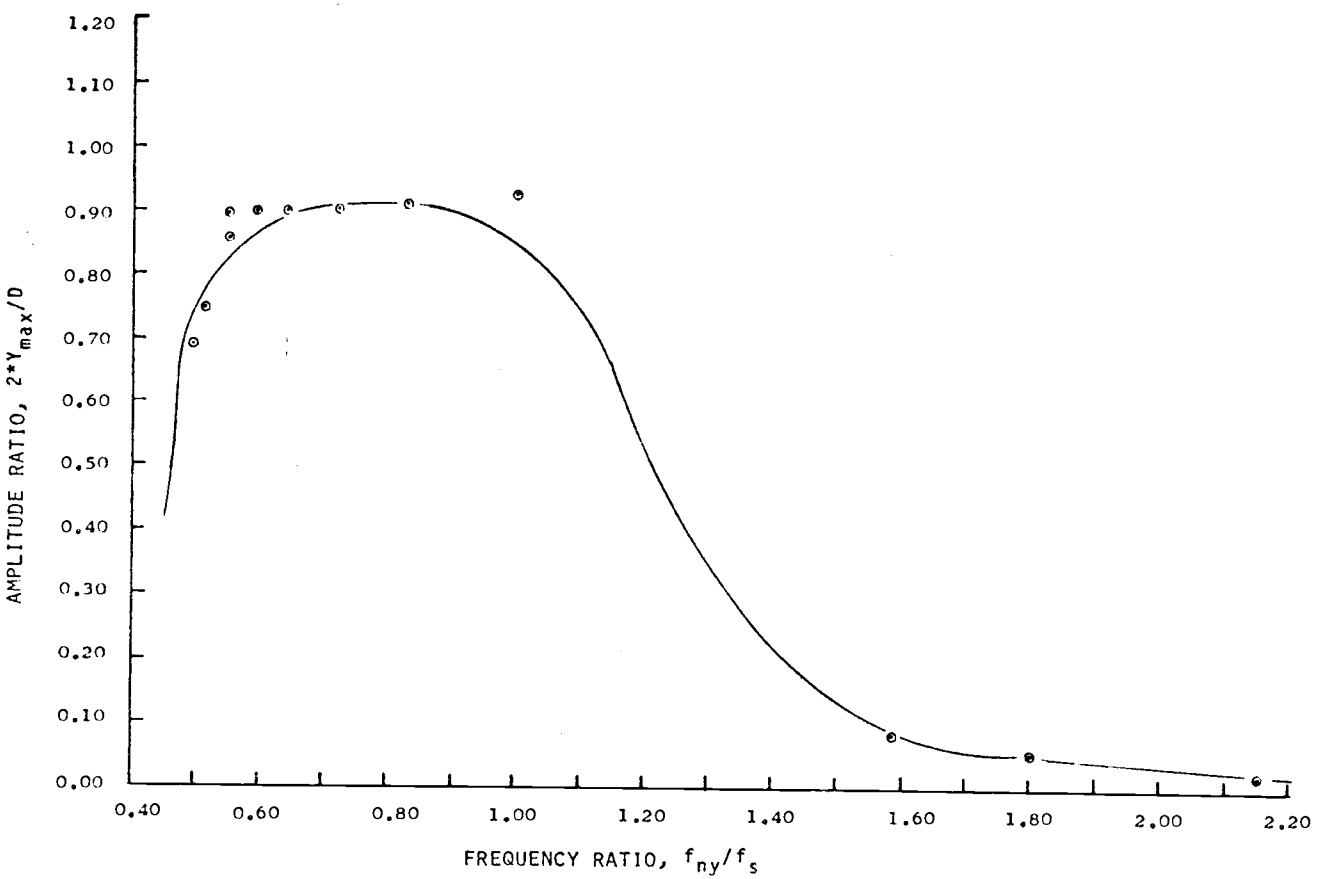

FIGURE 7. Peak-to-peak oscillation amplitude, run #20-10.5 .

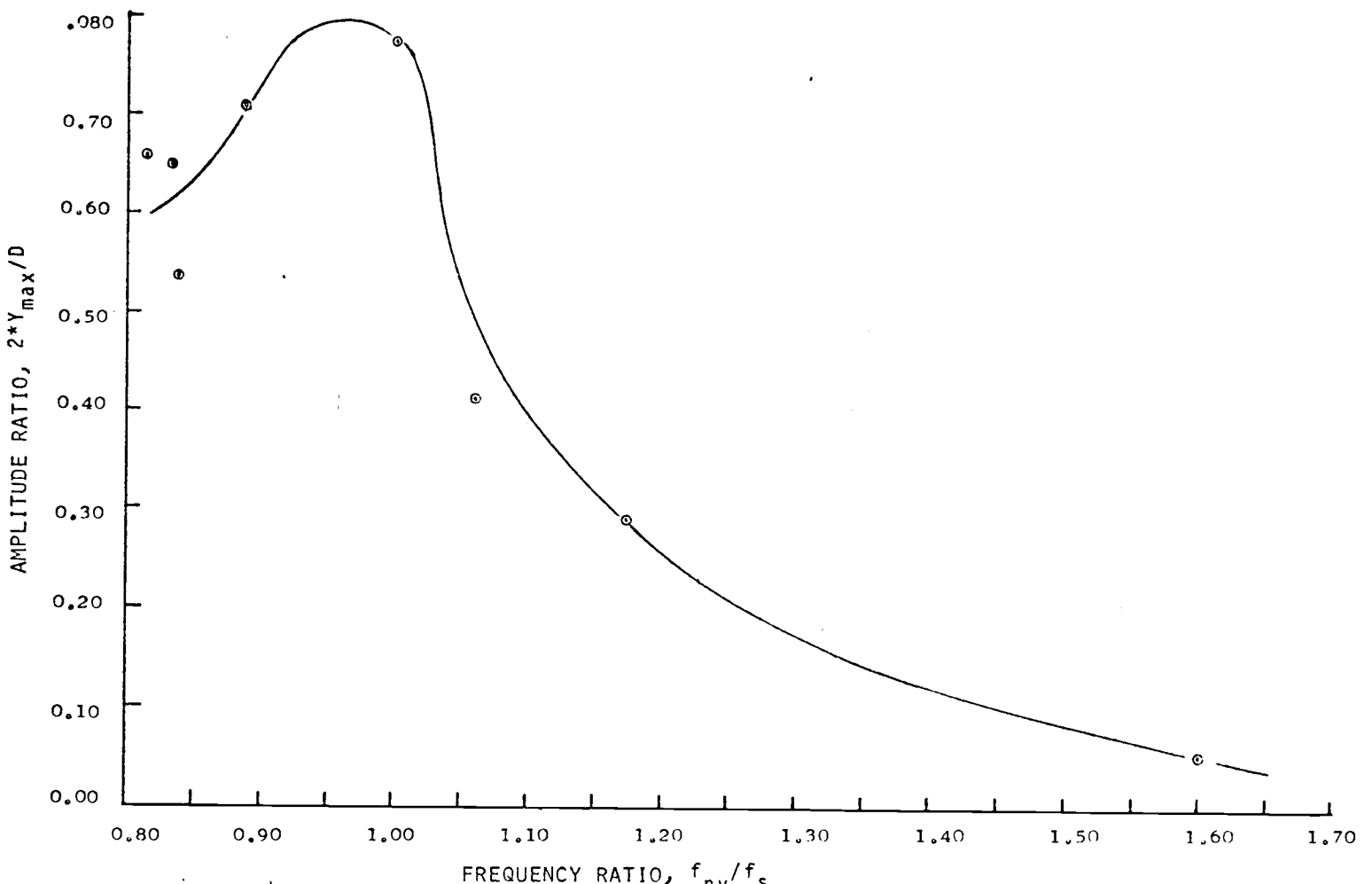

FIGURE 8. Peak-to-peak oscillation amplitude, run #20-20.5 .

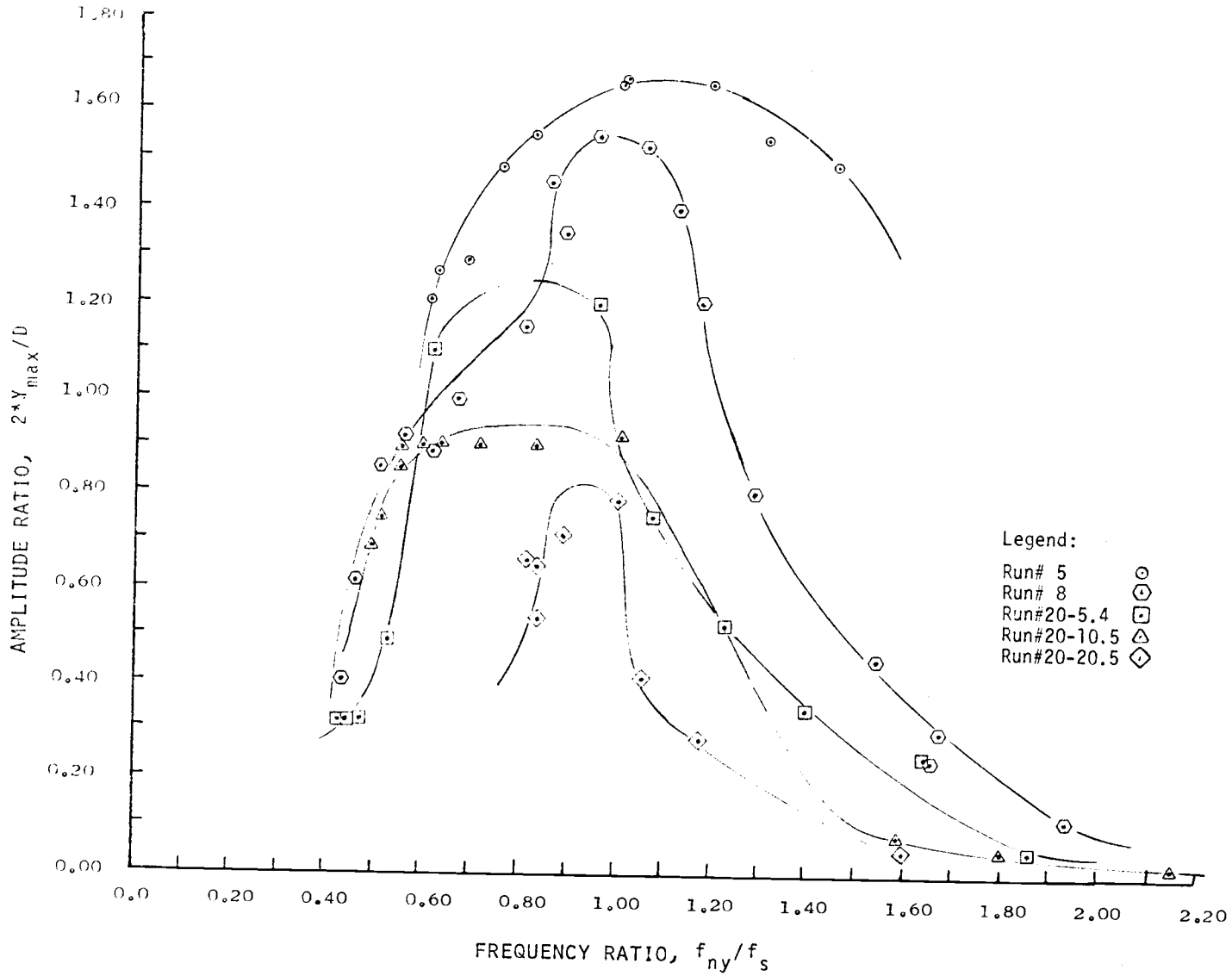

FIGURE 9. Summary of peak-to-peak oscillation data.

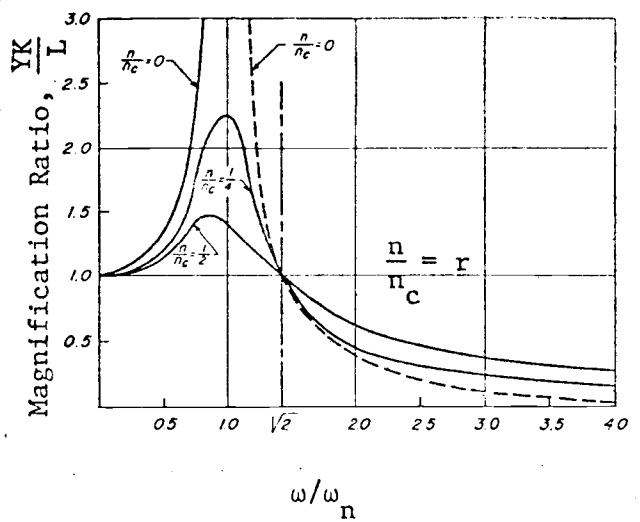

FIGURE 10.

Common linear second order response curve

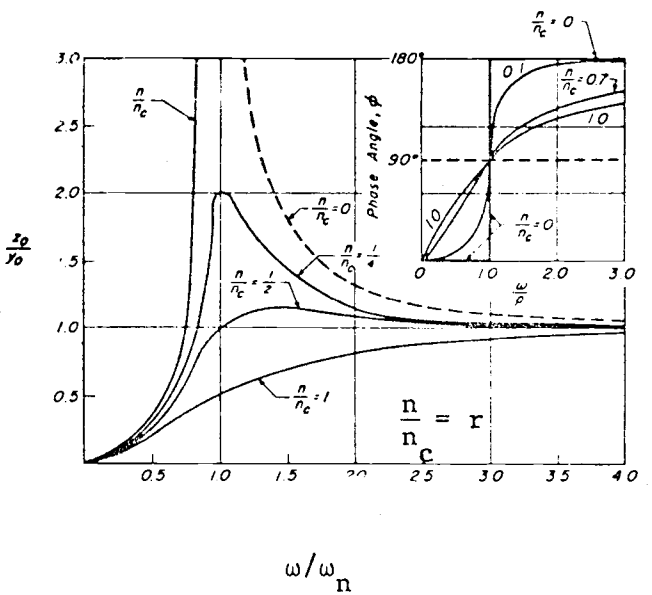

FIGURE 11.

Common linear second order amplitude ratio curve

system. The apparent damping ratio for each of the systems was determined on the basis of the aforementioned "pluck test" and the calculated undamped natural frequency ω_n. The damping ratio and other pertinent parameters and equations are listed as a part of the tabular data shown in Tables II, III, IV, V and VI.

Comparing runs 5 and 8, one observes that, for a given cable size and constant elastic constraints, the lighter cable is more responsive to the exciting forces since it shows a greater amplitude and oscillates at large amplitude over a greater range of frequencies. The author speculates that had models been tested which duplicate the weight per foot of comparably sized manila and synthetic ropes (0.5 to 0.9 lb/ft for 1-3/4 inch diameters), even higher and perhaps wider response curves would have been observed. Limitations on the minimum combined weight of the cross-carriage and cable model and upon the force measuring transducers employed prevented the modeling of rope weight cylinders with the apparatus used here.

A comparison of the amplitudes of runs #20-5.4, #20.10.5 and #20-20.5 indicates that the peak amplitude is evidently some inverse function of stroke length, since the only thing that differs between these runs is the length of stroke for the harmonic driving motion. Figure 12 is a dimensionless plot of the peak response for run #20 as a function of stroke length. This result appears contrary to what the author had expected. Examination of the works of Laird (9 &10), Dale (4), Cassarella (3), Havelock (6), Bidde (2) and others gives neither evidence to support or refute this observation. Needless to say, more experiments specifically aimed at this apparent paradox should be

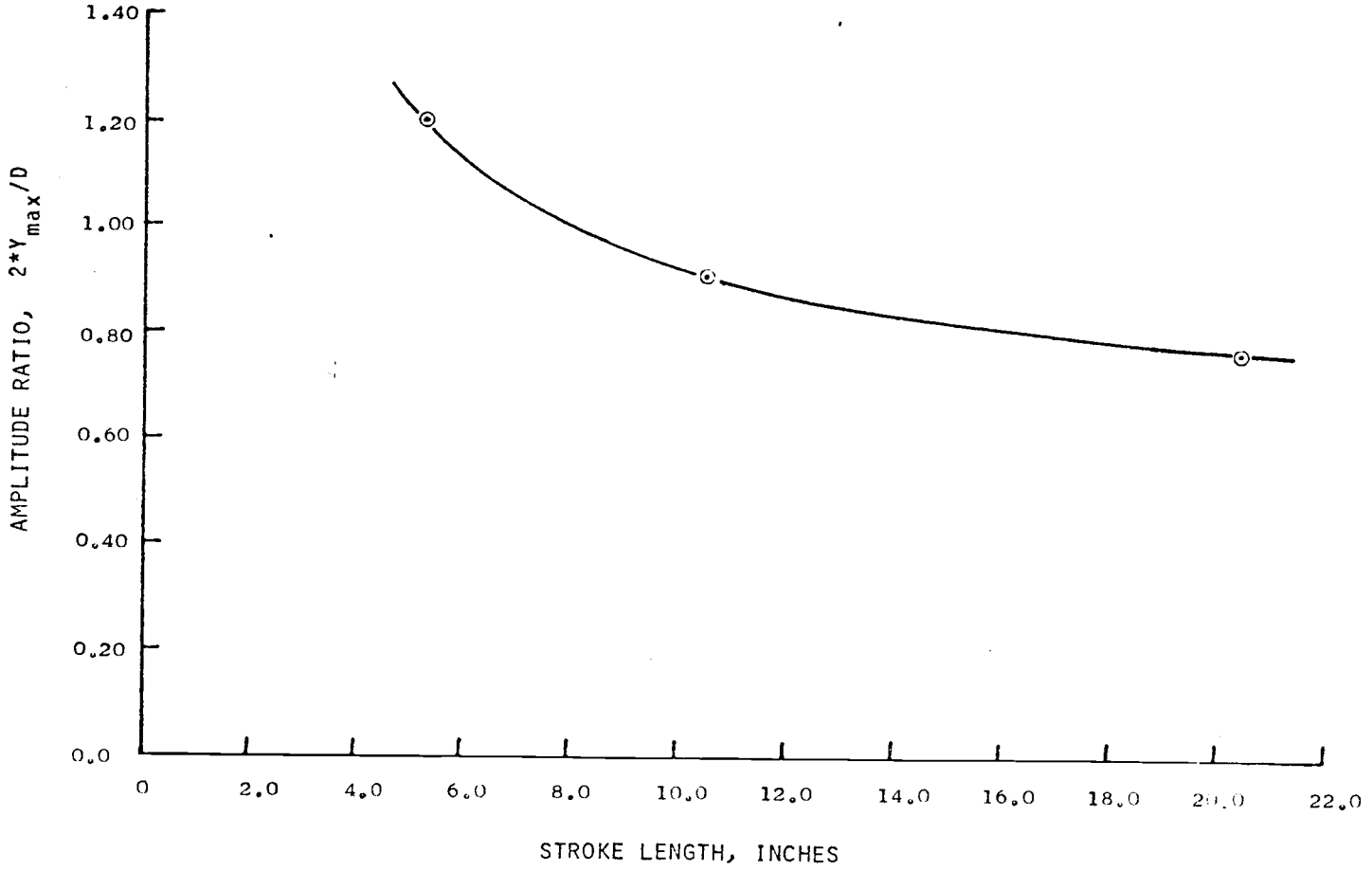

FIGURE 12. Peak response amplitude and stroke length.

performed before one becomes comfortable with this observation. In general, the response curves shown herein are clearly more definitive than any produced up to this time though these curves themselves leave much room for expansion and improvement.

The reader should note that the Strouhal frequency, Reynolds Number, F_{xmax} and F_{xmin} are all calculated on the basis of the peak applied harmonic velocity. The reason for this was to facilitate comparison with the works of Laird (9 & 10). If the reader wishes, he may modify the results by a suitable scale change on the graphs to use X average or X RMS.

The lower oscillograph trace on Figure 13 shows a high frequency oscillation (f_x) approximating a harmonic form together with an oscillation whose frequency equals the driven frequency of the applied harmonic motion X. The magnitude of f_x is approximately twice the lateral exciting frequency f_y which in turn approximately equals the Strouhal frequency f_s. The corresponding trace of f_y is shown below the upper curves for comparison. Laird (9 & 10) also observed a similar relation between f_x and f_y. The exact ratio between these frequencies appears to be somewhat dependent upon the stiffness of the lateral constraints of the cable model. According to Laird (10), stiffer constraints give oscillations in both X and Y directions which approach the natural frequency of the cylinder. In this series of experiments, no springs stiff enough were used to substantiate these findings one way or the other.

Figure 13 will help the reader understand the meaning of the unsteady drag terms used in Figures 14, 15, 16, 17, 18 and 19. It should

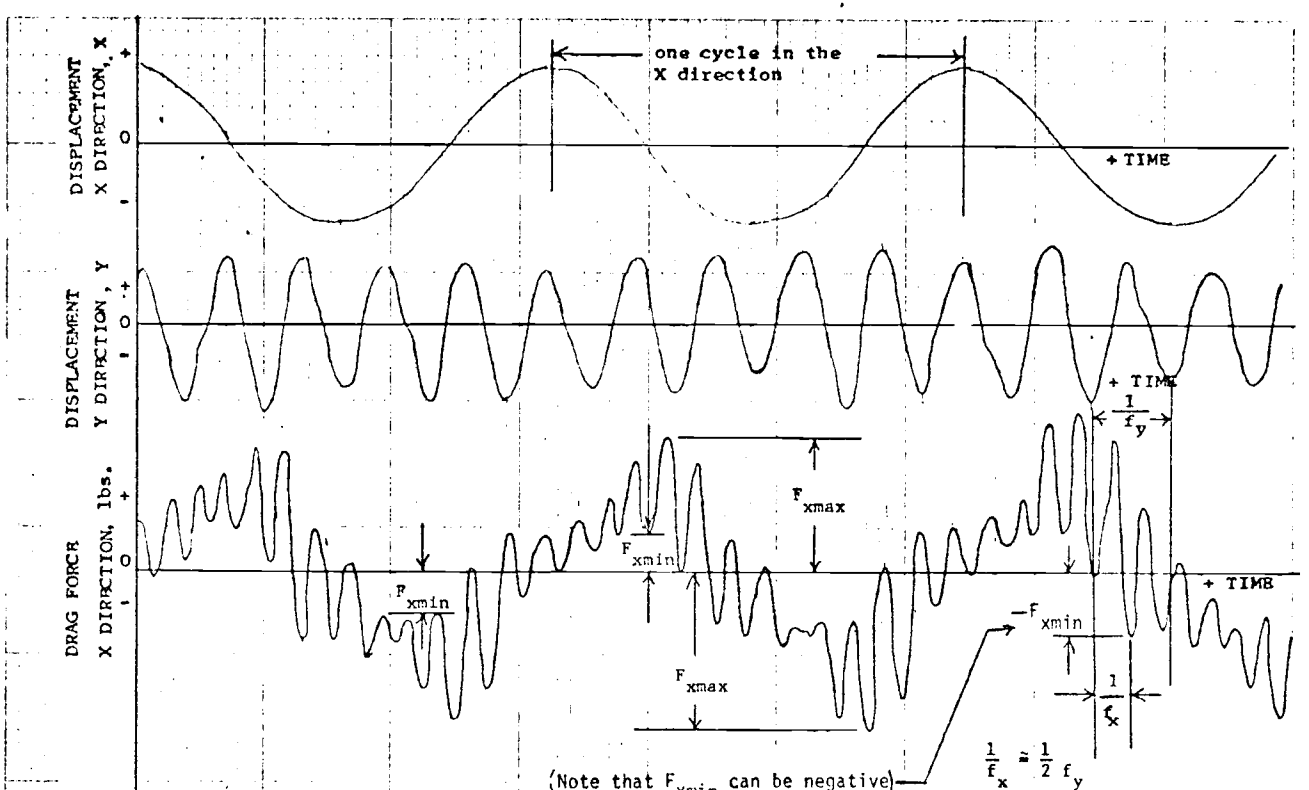

FIGURE 13. Trace of typical oscillograph plot.

be noted that the values shown for F_{xmin} are not the minimum values of the drag force ratio observed during any one cycle, but the minimum value of the drag force ratio occurring around the time when the velocity was maximum. The drag envelope curves were constructed to facilitate comparison with the hydrodynamic drag that would be predicted using the common equation and drag coefficient (drag force = $F = \frac{1}{2} C_d \rho A V^2$) normally used for rigidly constrained cylinders.

The drag envelope curve showed no marked bell shaped curve corresponding to the peak values of the amplitude ratio shown in Figure 9. This was not too surprising in light of the findings of Laird (9 & 10) and Dale (4). Laird tried to relate drag forces to wake widths and Dale compared drag forces with a "virtual diameter" based on the effectiveness in blocking the flow of the strumming cylinder. Both of these approaches are quite similar and both showed poor correlation with either of the variables. While Laird's work was primarily directed toward pilings in an oscillating flow, the results are certainly similar to those obtained here. The maximum observed drag force ratios observed by Laird were on the order of five while ratios slightly over seven are shown here. The natural frequencies, cylinder size and stroke length were comparable in both cases, though Laird's apparatus was constrained differently in the direction of applied harmonic motion.

Figure 19 facilitates comparison of the various drag envelopes. The apparent scatter of the data is very typical of that shown in References 2, 4, 8, 9, 10 and 14. One possible explanation for some of the apparent scatter and irregularity of the points on each of the

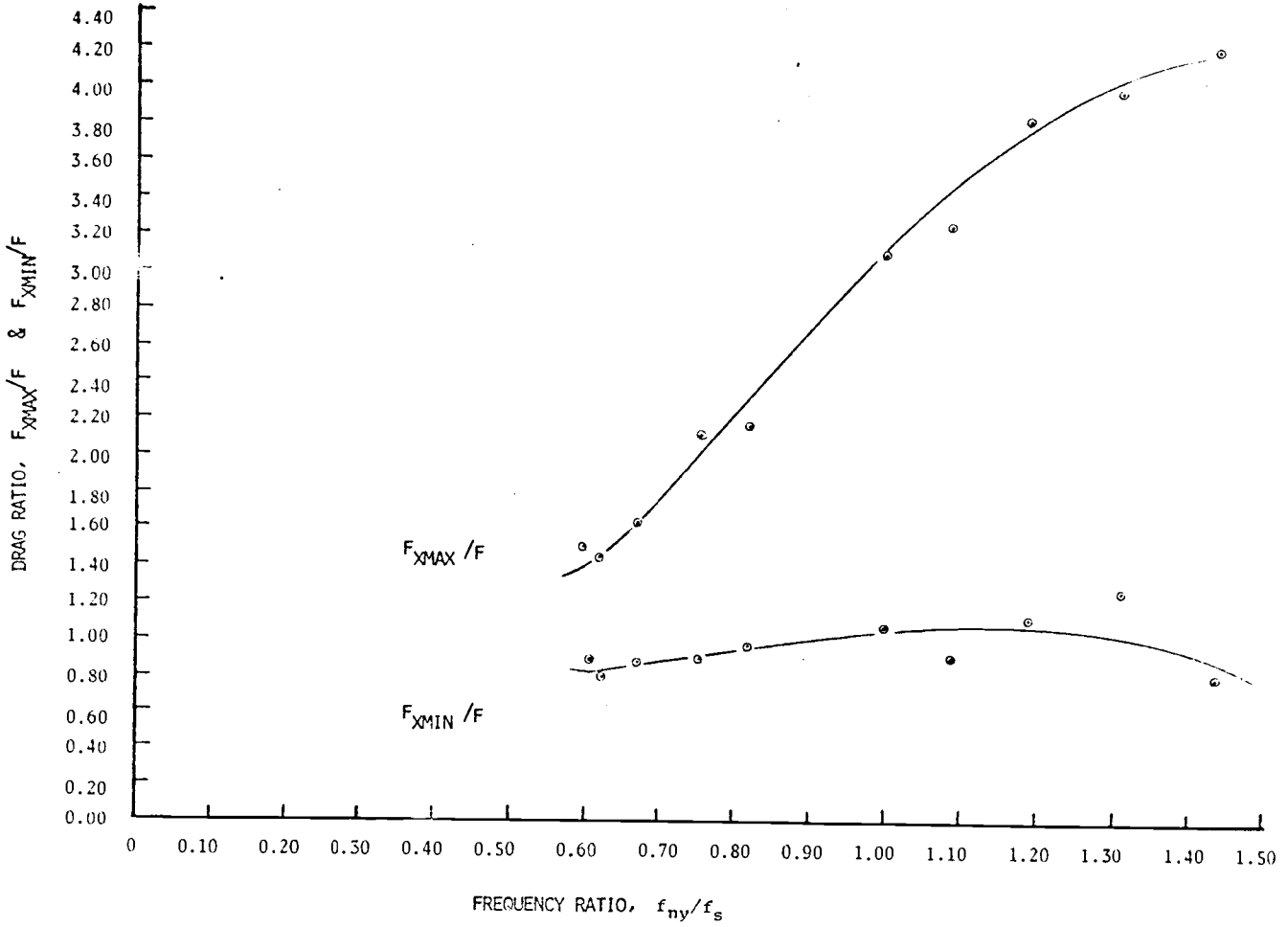

FIGURE 14. Drag envelope, run # 5.

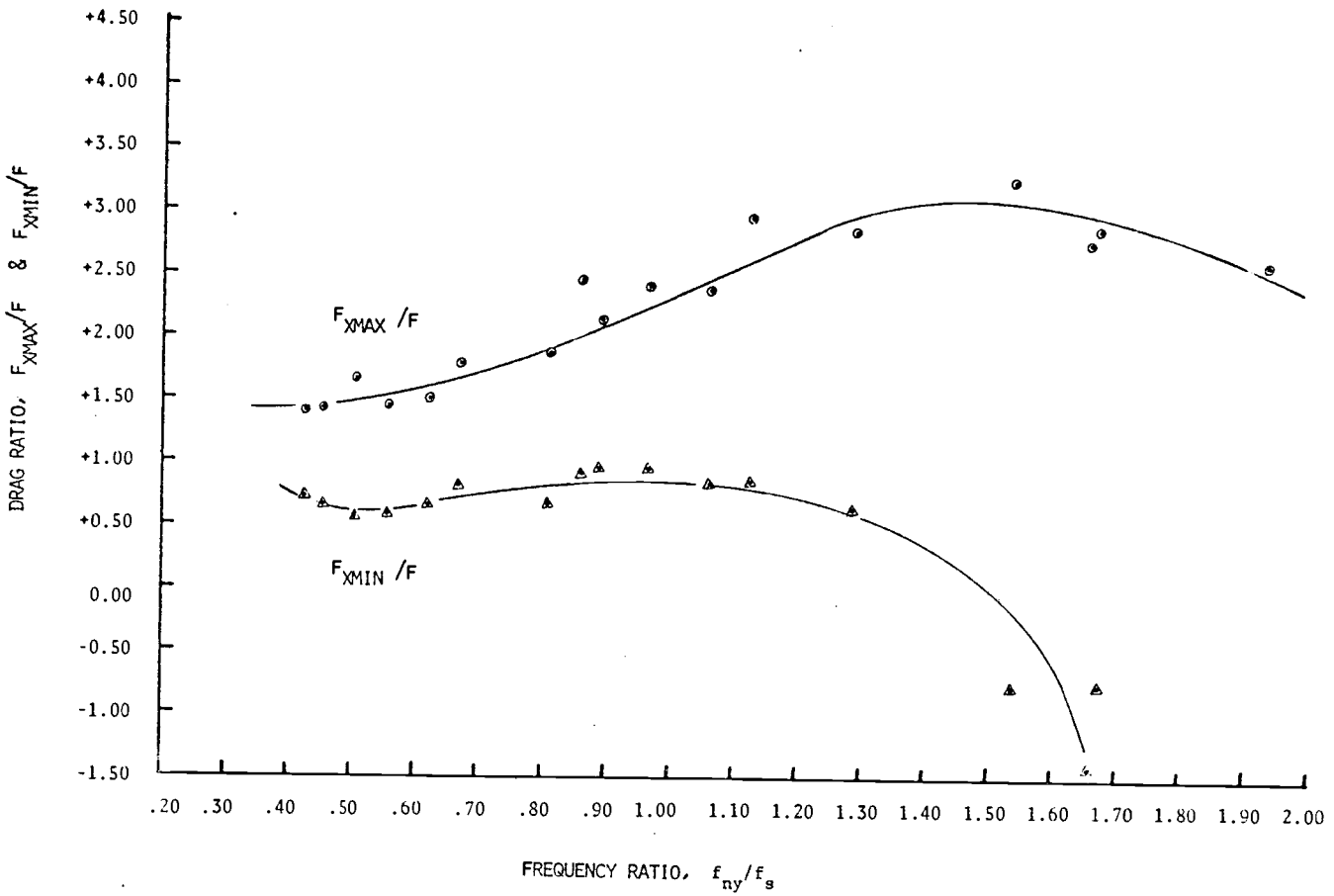

FIGURE 15. Drag envelope, run # 8.

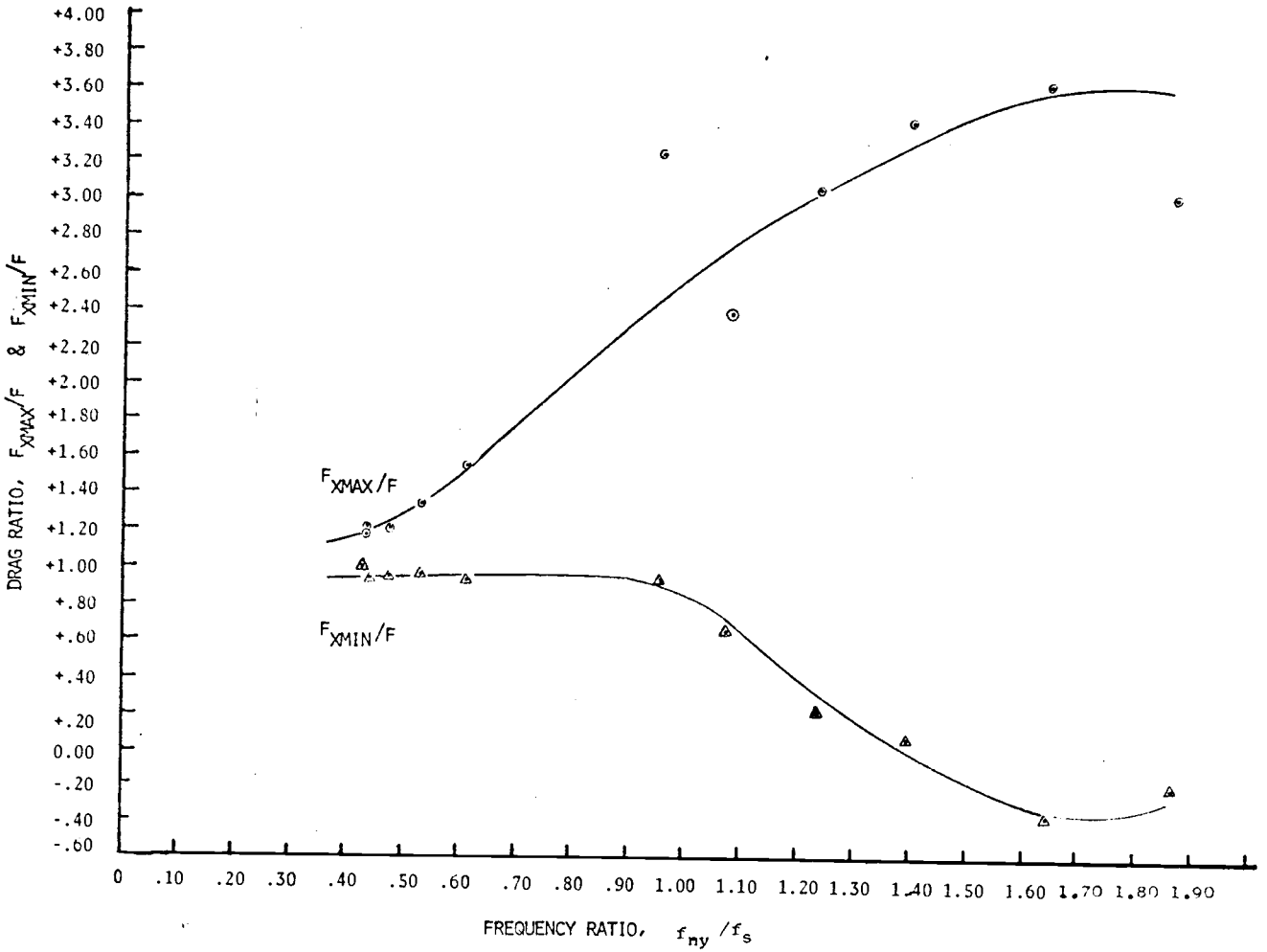

FIGURE 16. Drag envelope, run # 20-5.4 .

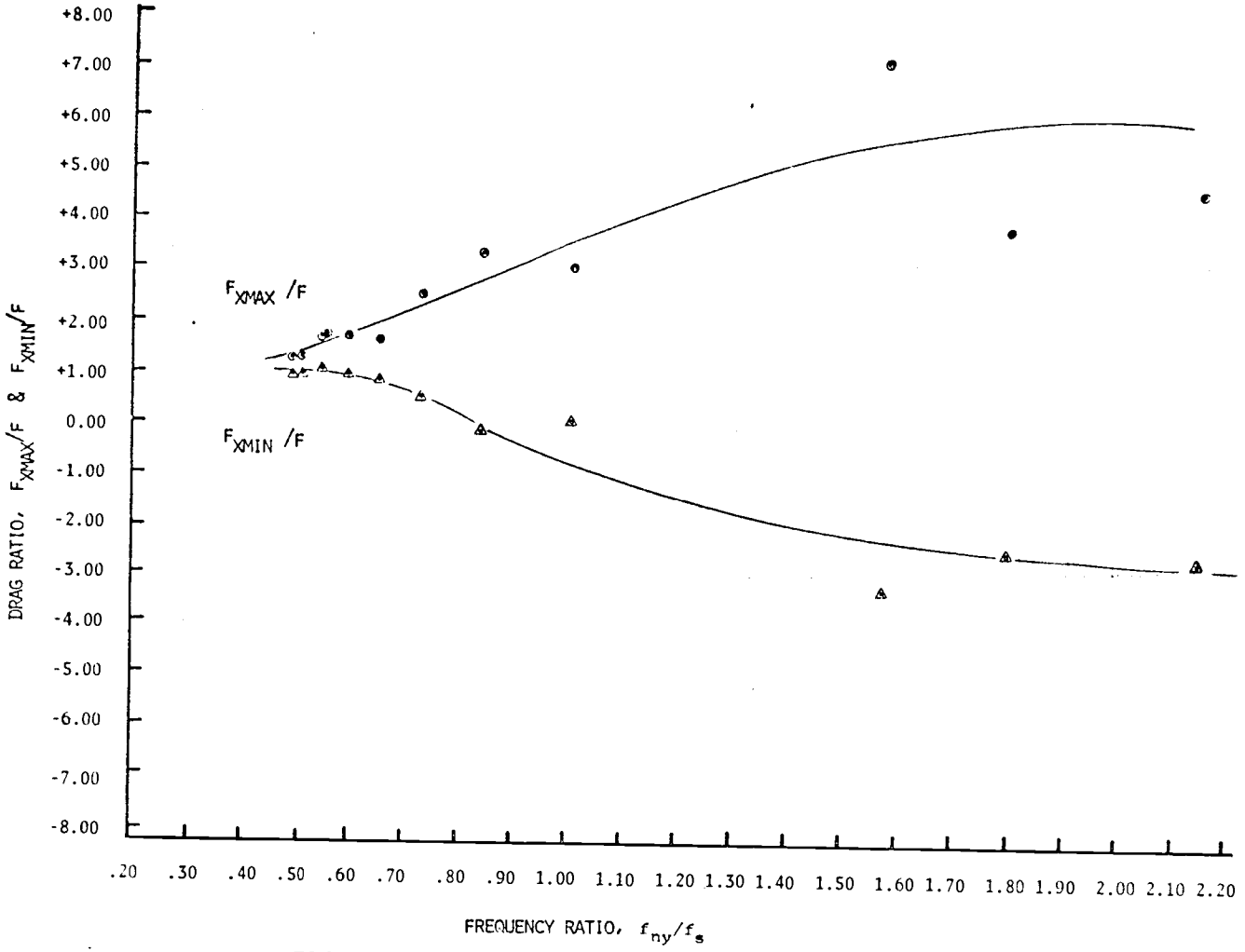

FIGURE 17. Drag envelope, run # 20-10.5 .

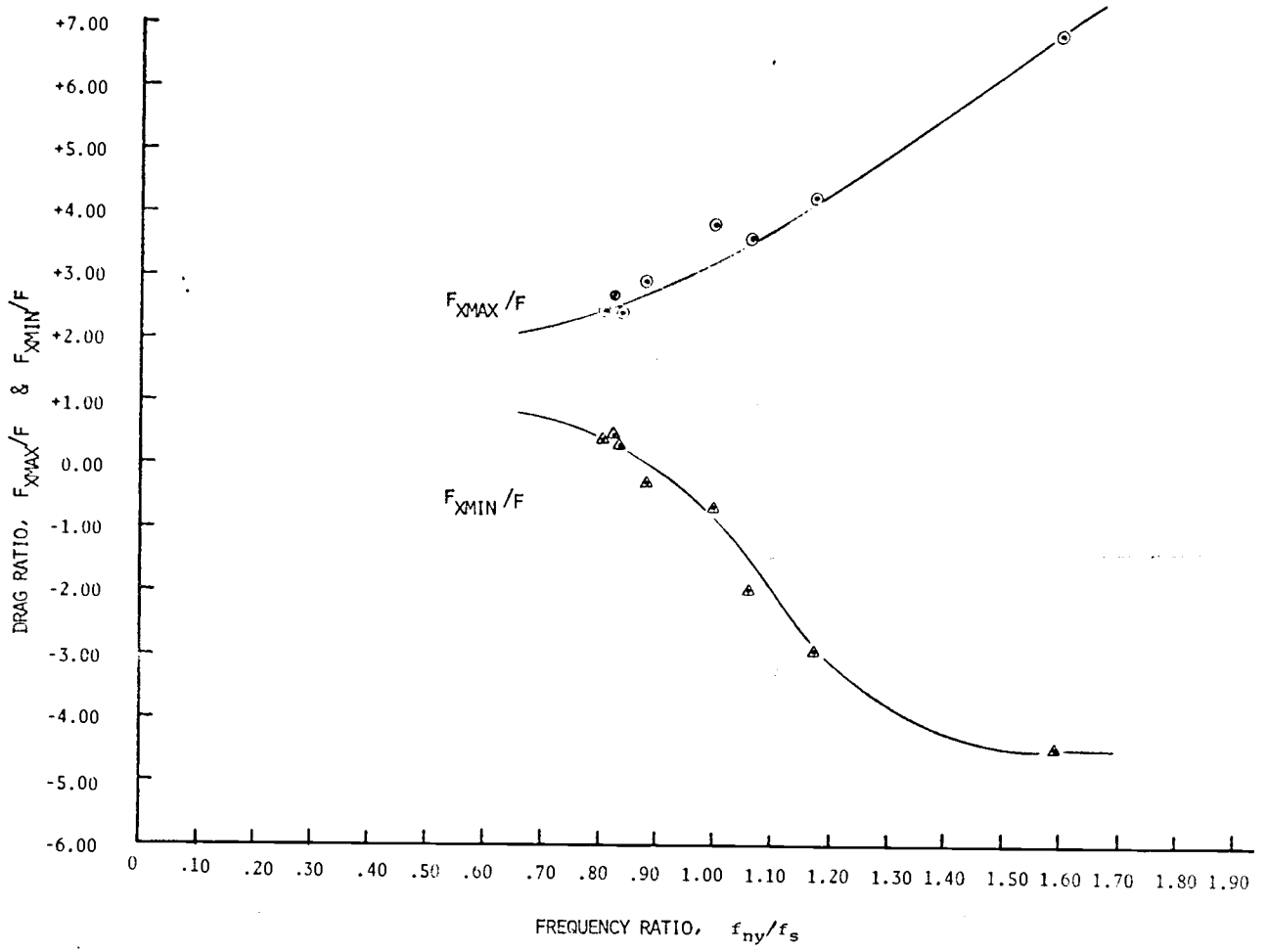

FIGURE 18. Drag envelope, run # 20-20.5 .

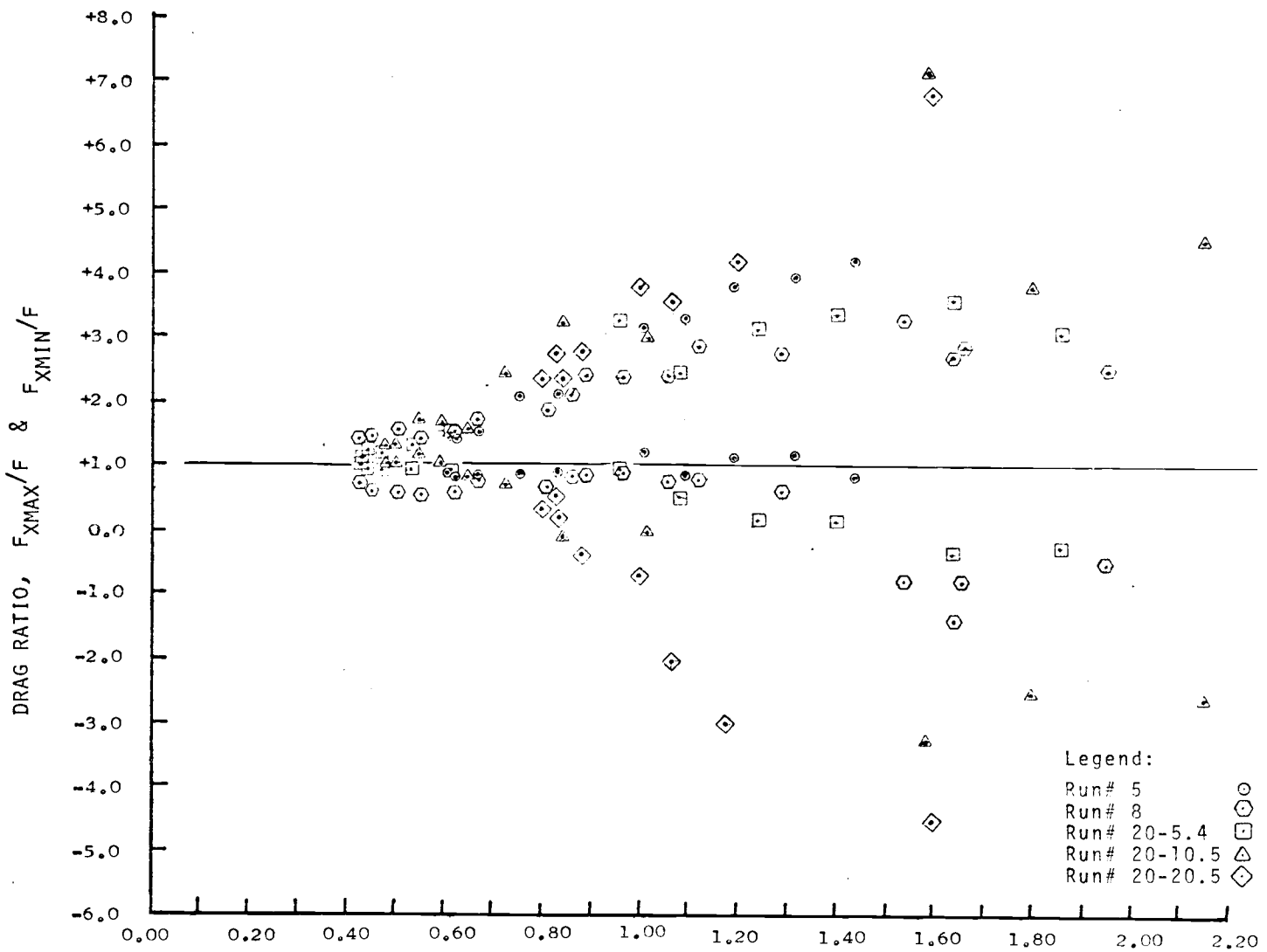

FIGURE 19. Summary of drag envelope plots.

graphs might be that the cable model was operating in a virtual sea of vortices shed during previous cycles. These vortices did no doubt cause some interference and complicate the apparent forcing function. However, not all of this variation can be blamed on previously shed vortices lying in the path of the cable. The irregularity of the raw data on the forcing function generated in still water indicated that the forcing function is considerably more complex than a velocity squared drag force and a harmonic function operating at the Strouhal vortex shedding frequency. The drag force is probably a function of time as well.

It is very apparent that the periodic drag force variations summarized in Figure 19 could, if duplicated by an actual system, lead to structural failure both by virtue of the peak loads applied and by virtue of failure due to exceeding the endurance limit.

The frequency variation curves (Figures 20, 21, 22, 23 and 24) were plotted to give some insight into the relation between the actual frequency (f_y) of oscillation (which must equal the effective forcing frequency or the true average vortex shedding frequency) and the Strouhal vortex shedding frequency as defined by equation (1). Figures 25, 26, 27, 28, 29 and 30, though not dimensionless plots, give even more insight into the phenomenon of "locking-in" than do their dimensionless counterparts described above. Previous experimenters have observed "locking-in" effects, where the cylinder has a marked tendency to oscillate at or near its natural frequency even though one might expect it to oscillate at the Strouhal vortex shedding frequency. The implication is that equation (1) is valid only for static cylindrical

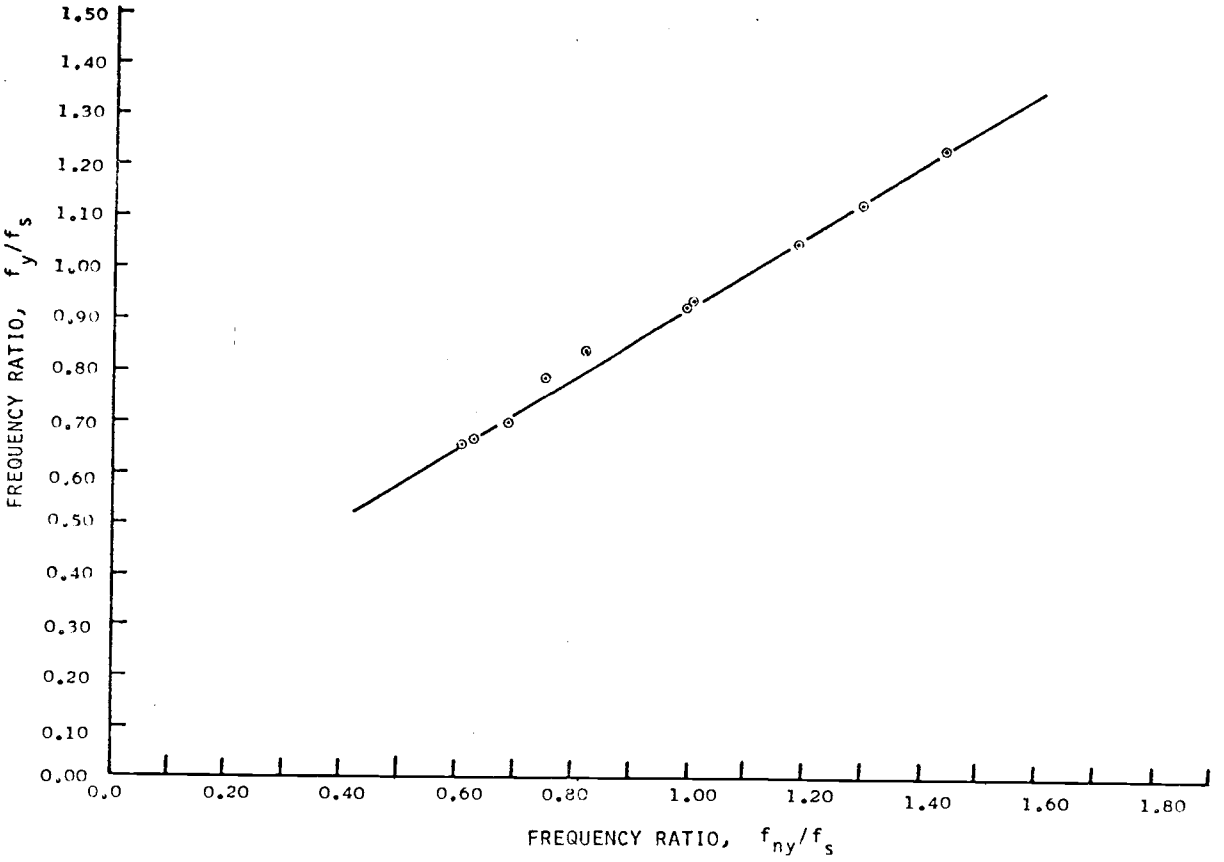

FIGURE 20. Frequency variation, run # 5.

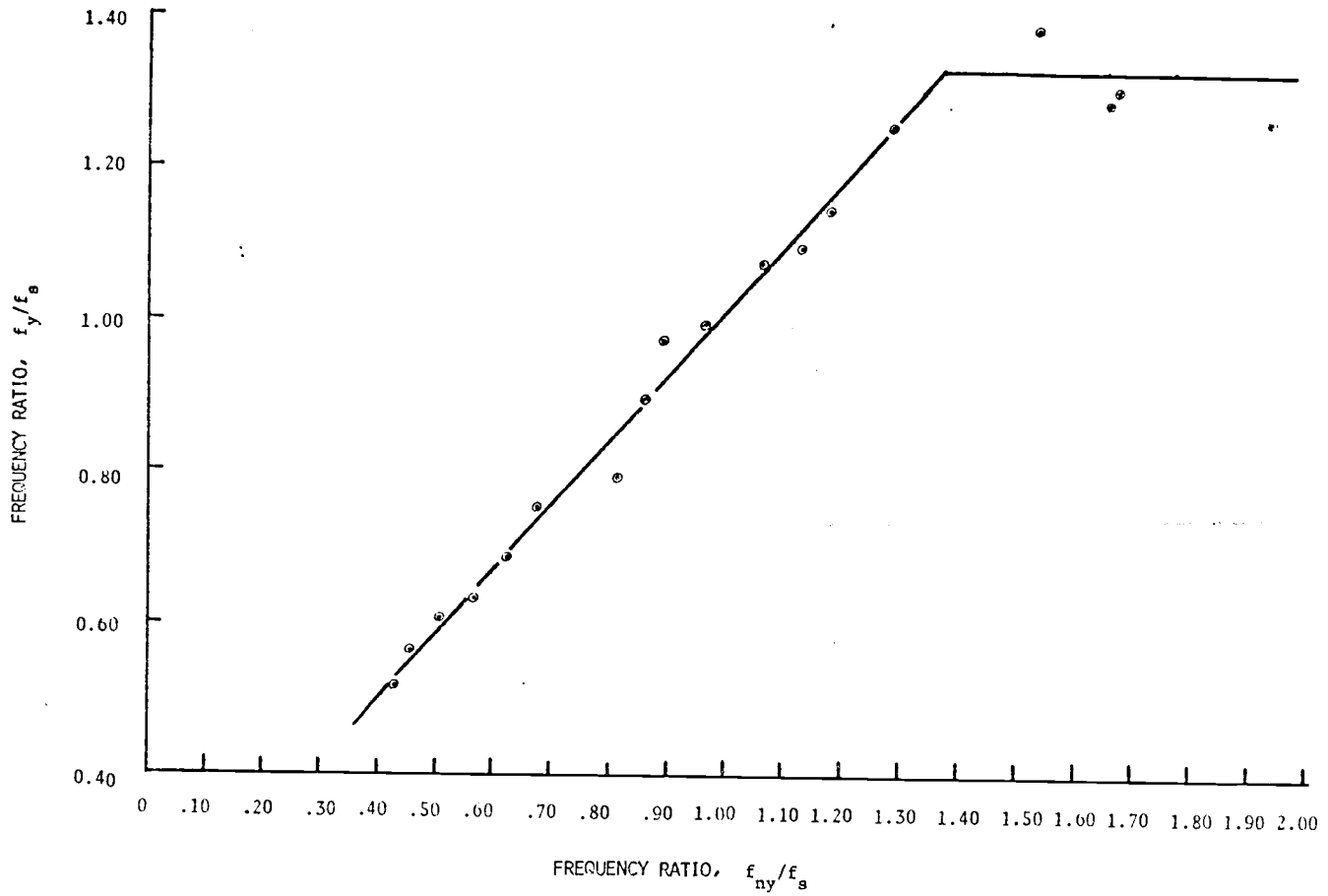

FIGURE 21. Frequency variation, run # 8.

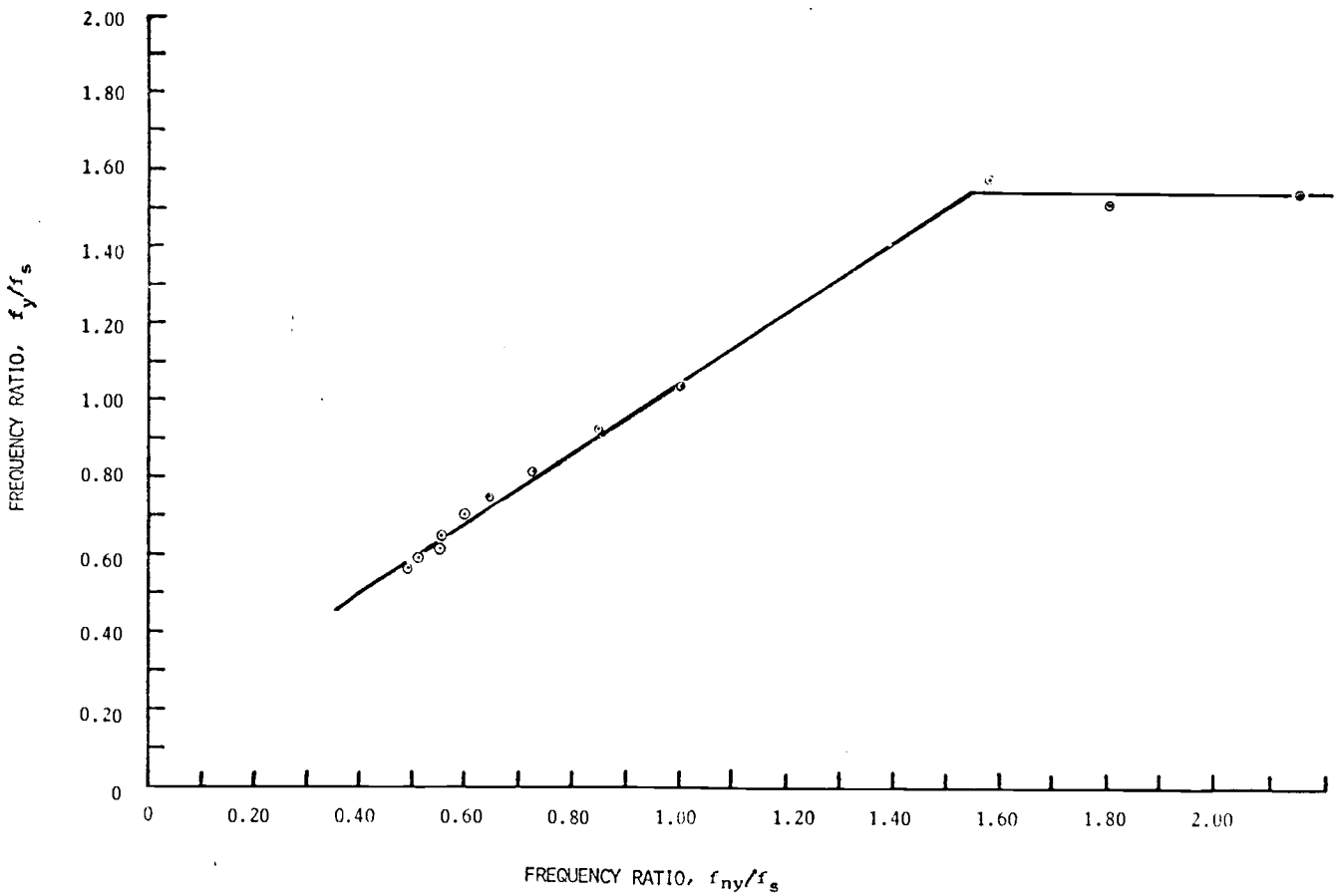

FIGURE 22. Frequency variation, run # 20-5.4 .

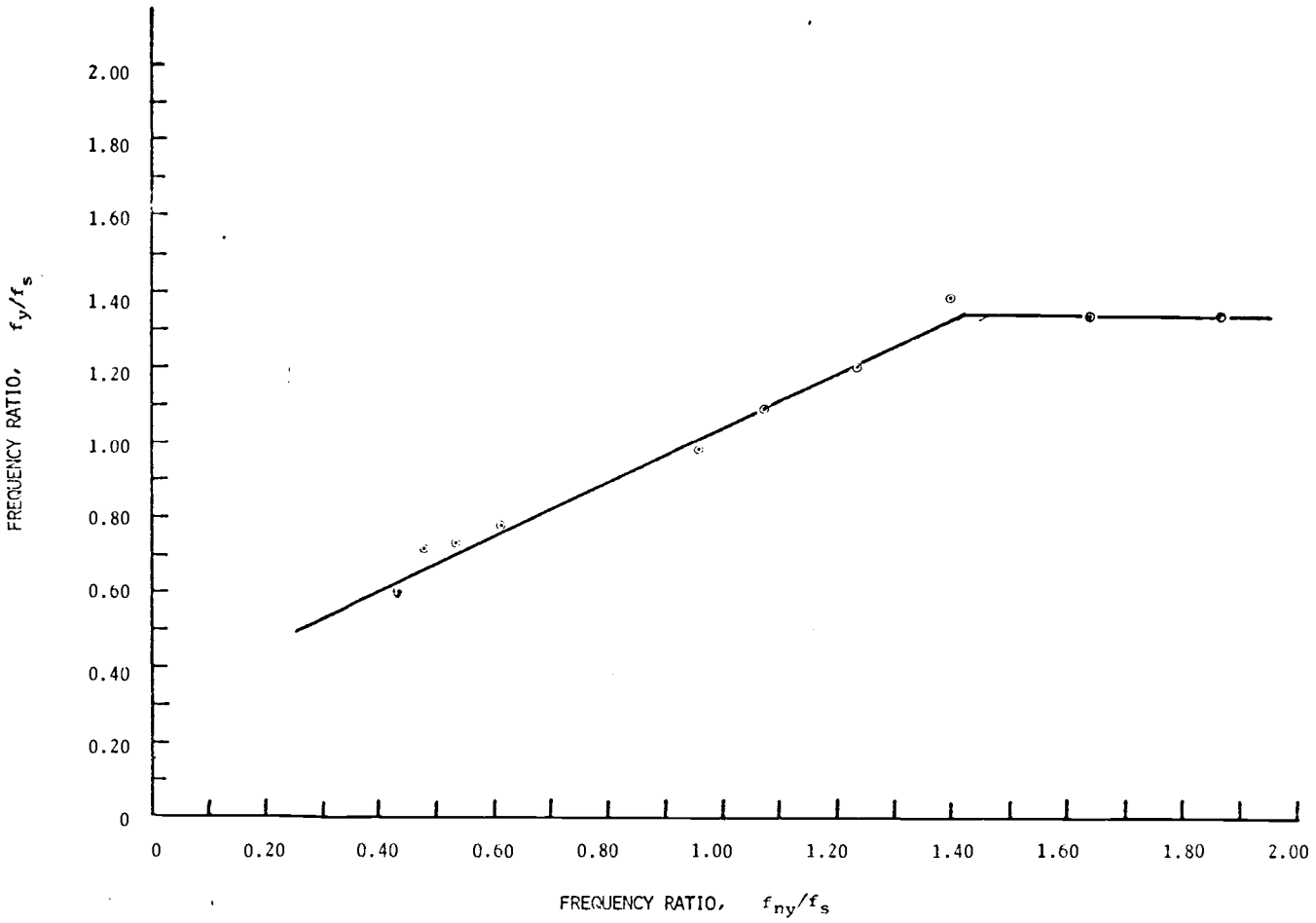

FIGURE 23. Frequency variation, run # 20-10.5 .

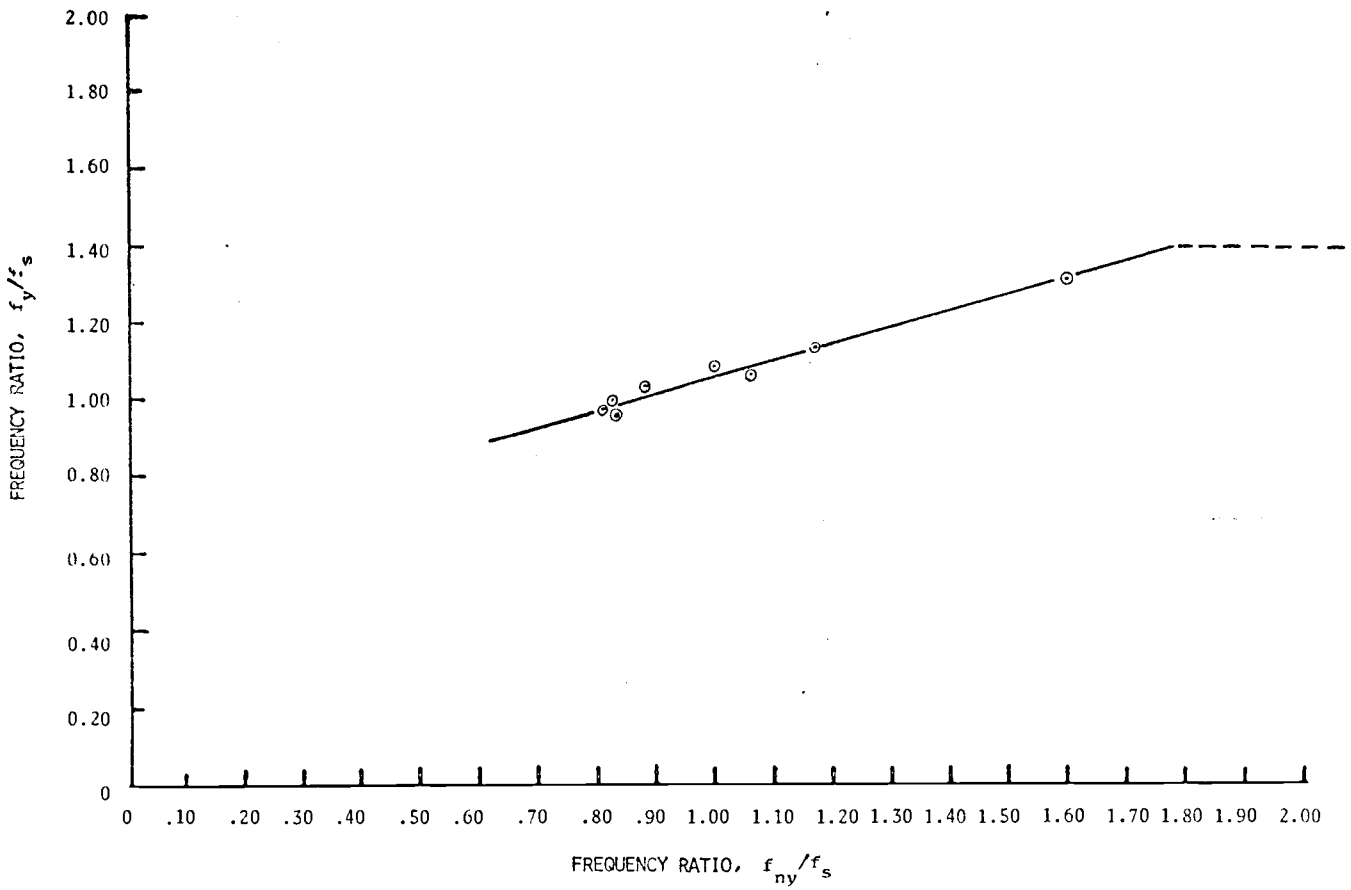

FIGURE 24. Frequency variation, run # 20-20.5

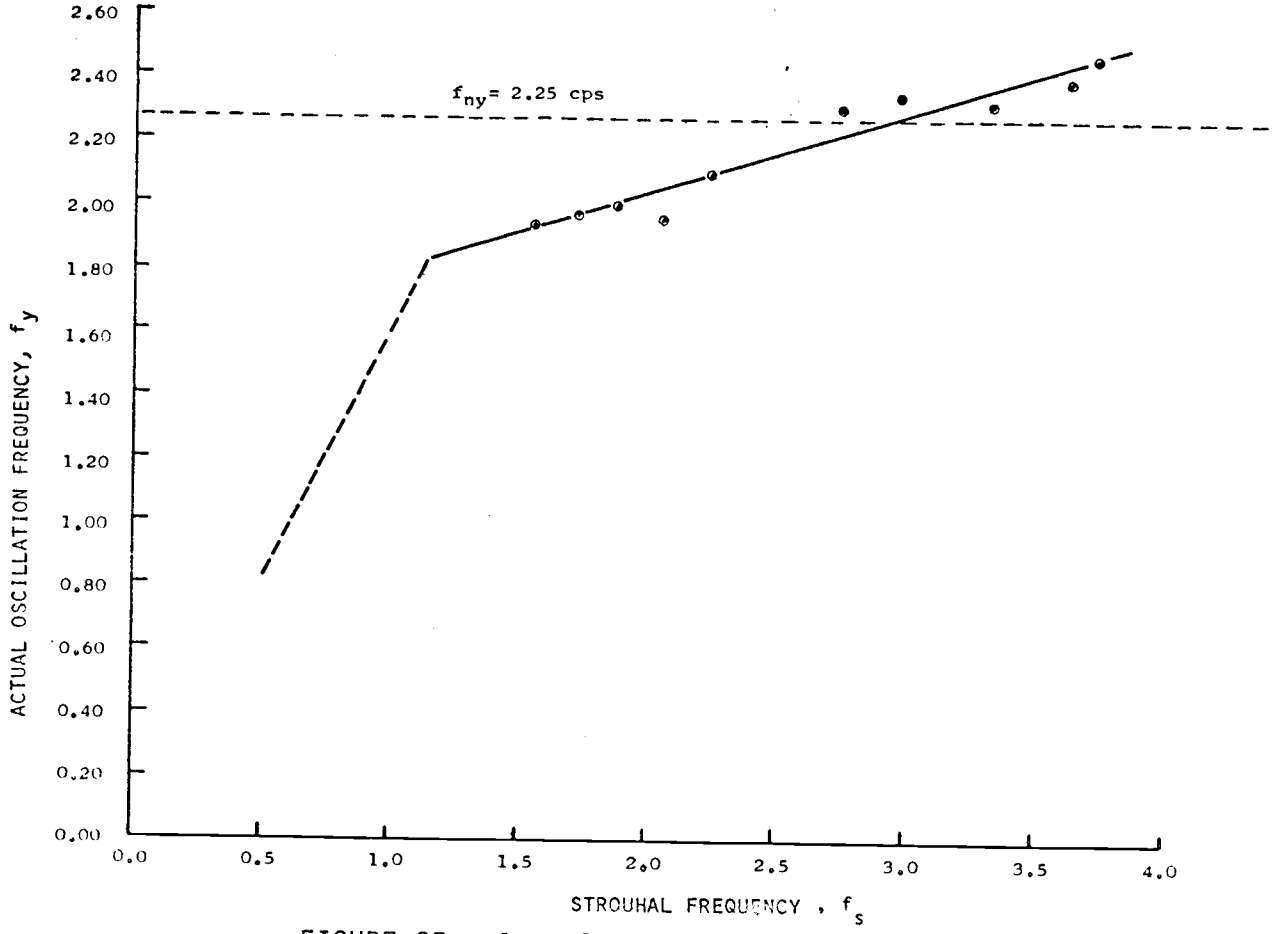

FIGURE 25. Actual oscillation frequency and expected exciting frequency, run # 5.

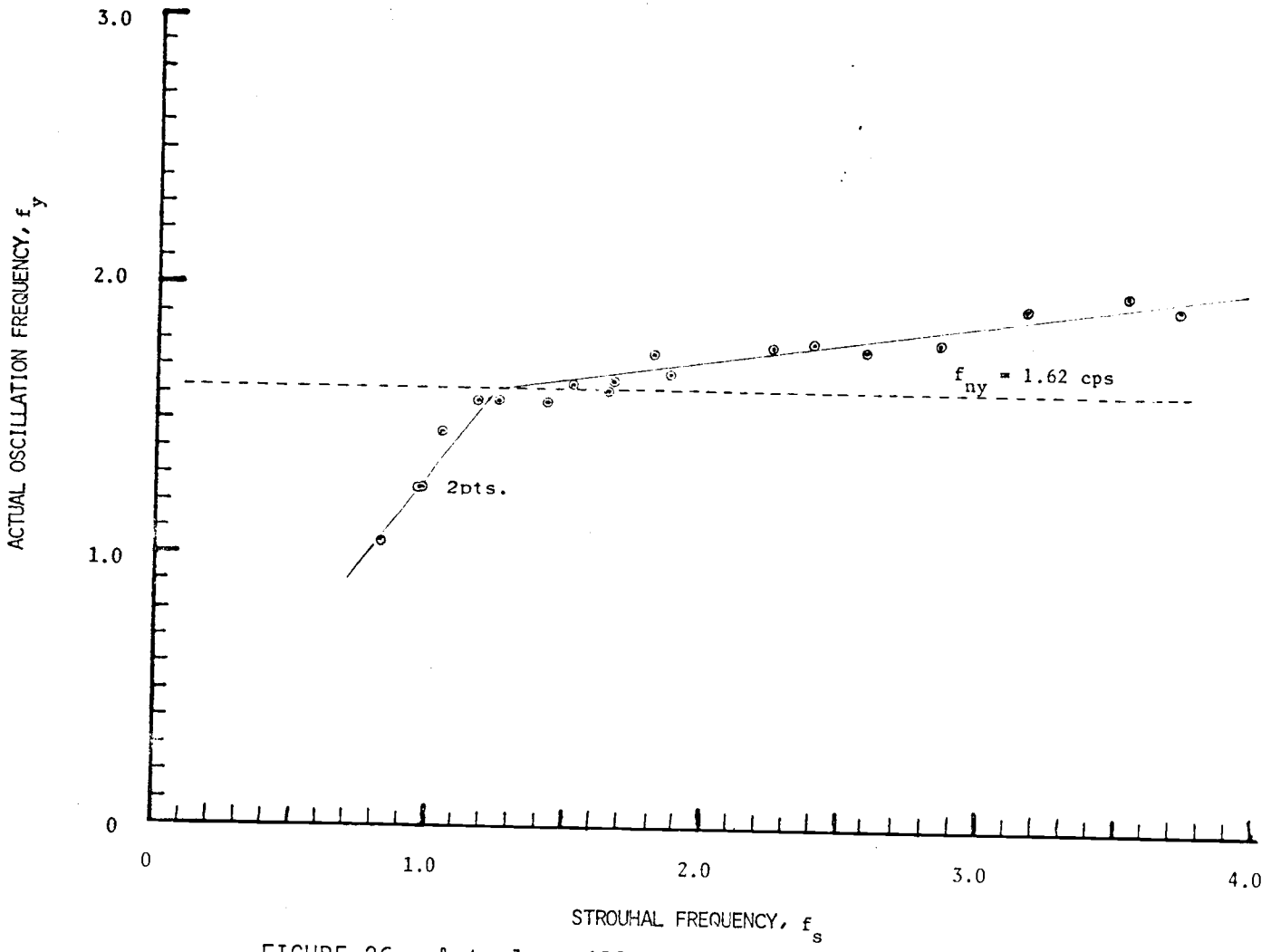

FIGURE 26. Actual oscillation frequency and expected exciting frequency, run # 8.

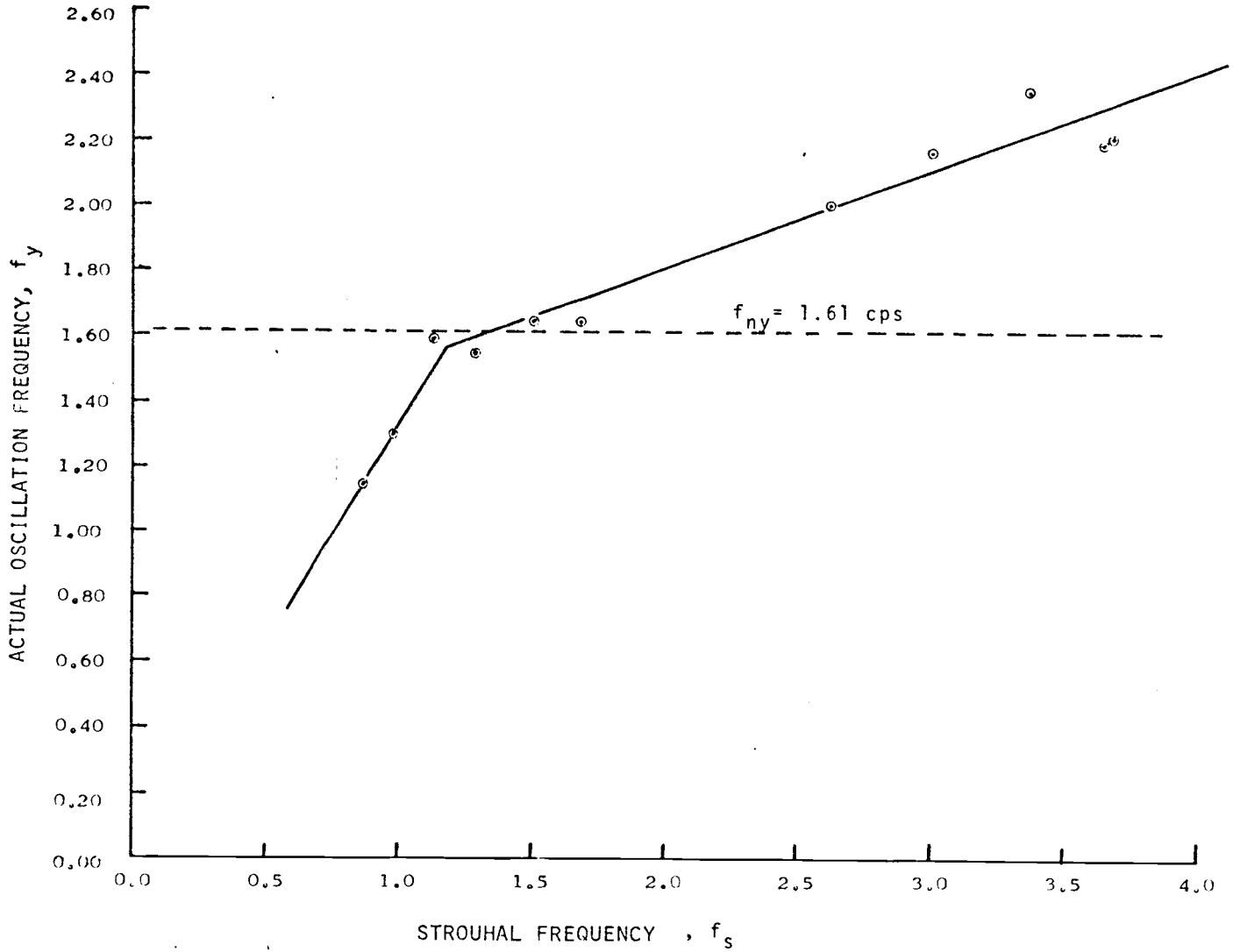

FIGURE 27. Actual oscillation frequency and expected exciting frequency, run # 20-5.4 .

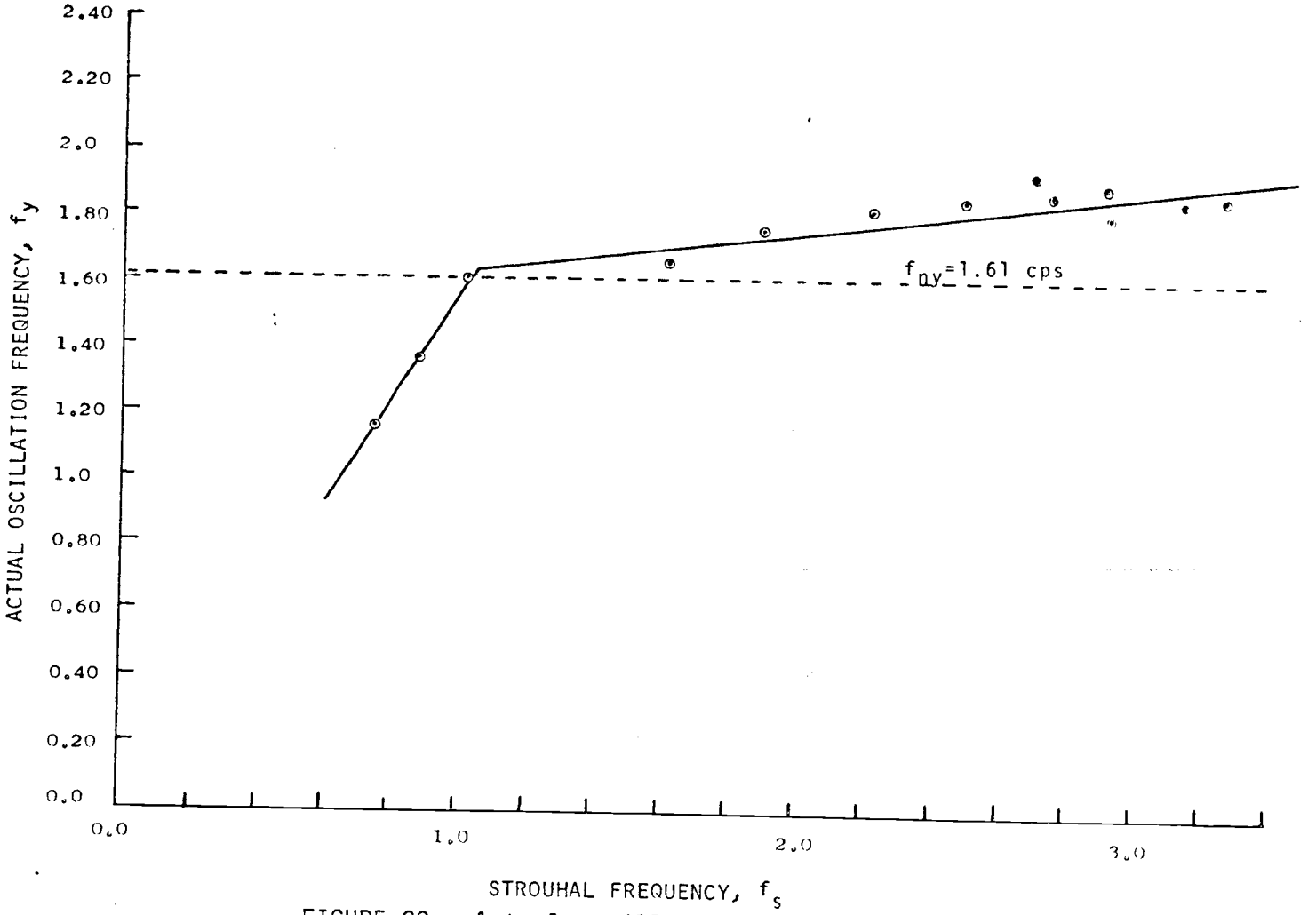

FIGURE 28. Actual oscillation frequency and expected exciting frequency, run # 20-10.5 .

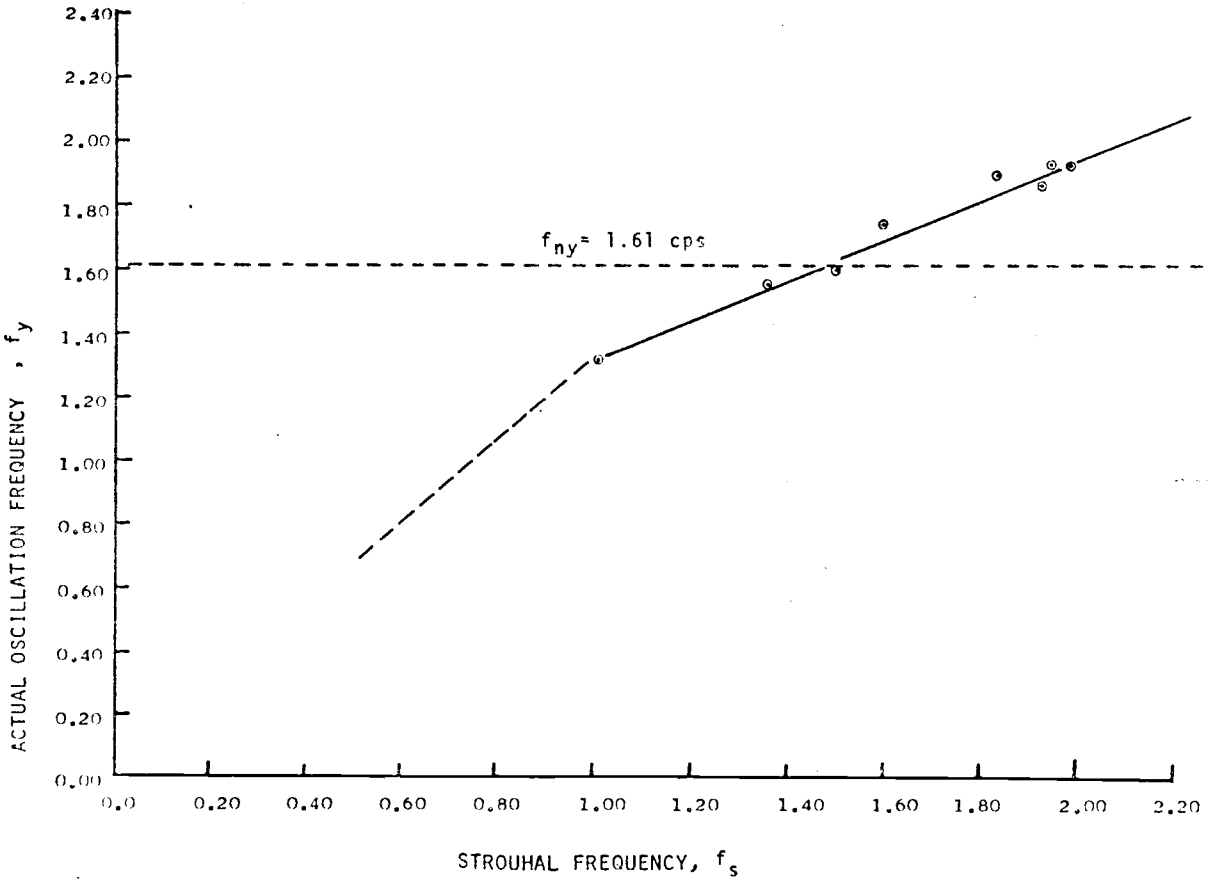

FIGURE 29. Actual oscillation frequency and expected exciting frequency, run # 20-20.5 .

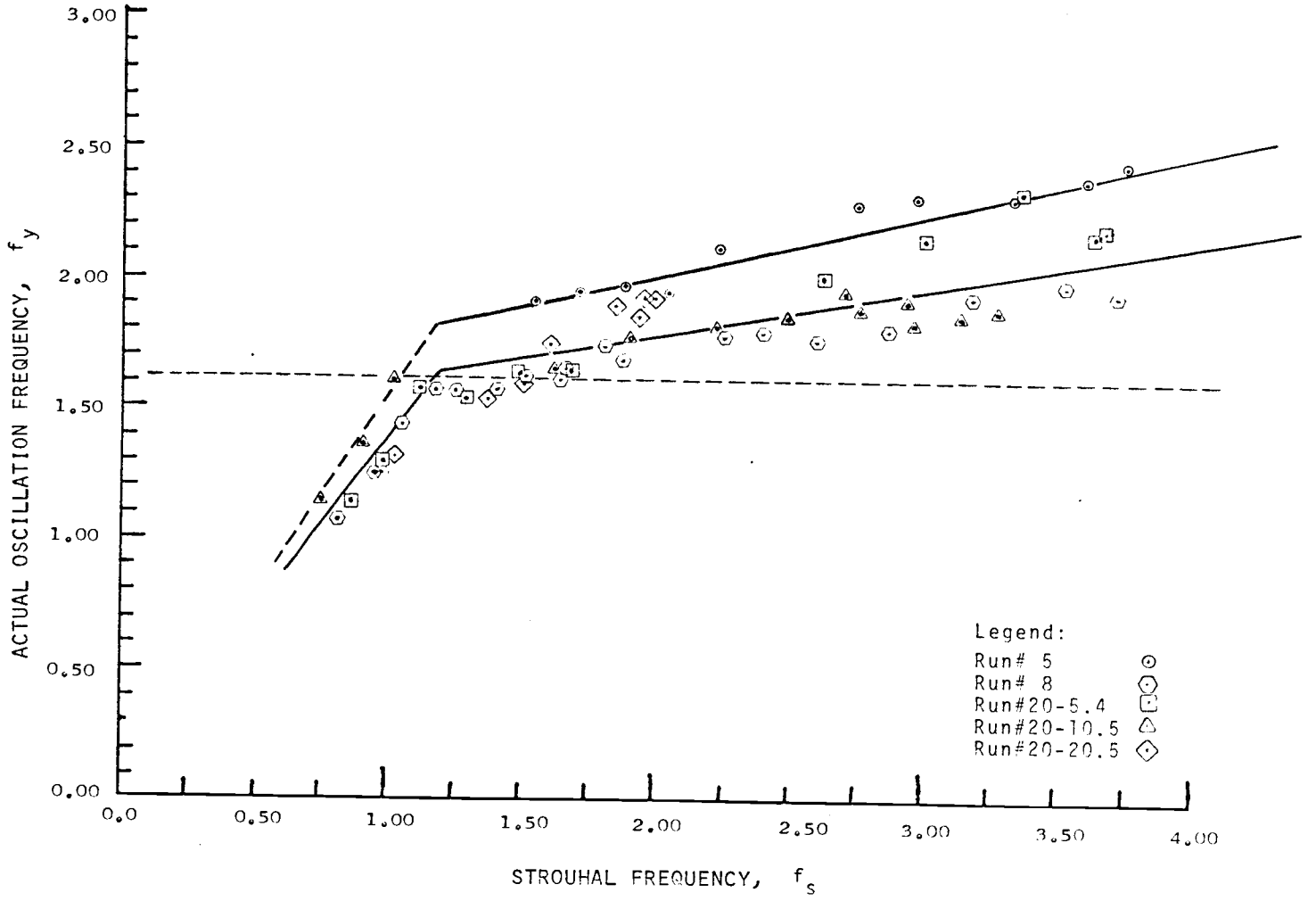

FIGURE 30. Summary plot of actual oscillation frequency and expected exciting frequency.

elements which are not free to move in either the X or Y directions. For a dynamic system, the true vortex shedding frequency is also a function of the frequency and amplitude of oscillation. Of the five plots of f_y and f_s, three (Figures 26, 27 and 28) show strong evidence to support the theory of "locking-in" or synchronization. Each of these plots show the Strouhal frequency f_s closely approximating the actual oscillation frequency f_y until which time resonance is reached ($f_y = f_{ny}$). The relationship between f_y and f_s appears to change near the point where the Strouhal frequency approaches the natural frequency and "locking-in" occurs. From this point on, the slope of the curves change almost as though the systems were following some forcing function which averaged the Strouhal frequency f_s and the system damped natural frequency f_{ny}. Figure 29 could be more conclusive in supporting the "locking-in" theory if the point opposite $f_s = 1.01$ did not fall as it did. Figure 25 gives even less evidence to support the "locking-in" theory because of the lack of a change in slope near the point where f_y equals f_{ny}. In spite of the aforementioned consistencies and inconsistencies, all five curves have nearly the same slope once beyond the resonance ($f_y = f_{ny}$) point. This can be best seen by a careful examination of Figure 30.

APPROXIMATE LINEAR EQUIVALENT SYSTEM

The actual equation which describes the transverse strumming of a cable is no doubt considerably more complex than the following equation, but the following equation does represent the system reasonably well.

$$(m' + m)\ddot{Y} + C_1\dot{Y}|\dot{Y}| + kY = \frac{C_2 A' \rho (\dot{X})^2 \sin(2\pi f_s t)}{2} \qquad (3)$$

The symbols m and m' are the actual and virtual masses of the cable respectively, and C_1 is a velocity squared damping coefficient. The equivalent linear spring constant or restoring force rate is given by k. The term on the right side is the forcing function which consists of the empirical constant of proportionality C_2, the projected area of the cable A', the fluid mass density ρ, the driven velocity $\dot{X}$, and the harmonic term whose frequency is the Strouhal vortex shedding frequency f_s. The term on the right is of the same form as a simple steady-state forward drag equation (drag = $\frac{1}{2} C_2 \rho A V^2$) with the constant of proportionality C_2 relating the coupling of drag forces in the X direction to the lateral exciting forces in the Y direction. The harmonic term was selected on the basis of observations of induced oscillations and photographs of Karman Vortex Streets similar to that shown in Figure 1. Other experimenters have concocted similar relationships. A second forcing function relating how the virtual mass (m') is related to $\dot{X}$ could also be added as a minor embellishment; but since this term was small and of unknown form, no attempt was made to add this term into the equation. This equation, which in itself is a

great simplification, can be further simplified to give the reader a better feel for the character of this phenomena. The linearized simplified equation is shown below.

$$m\ddot{Y} + C_3\dot{Y} + kY = L\sin(2\pi f_s t) \qquad (4)$$

All symbols are the same as in the preceding nonlinear equation (3) save C_3 and L which are respectively, the equivalent linear viscous damping coefficient and the equivalent forcing term. This forcing term L will make the cable model oscillate at essentially the same amplitude as the average amplitude shown in the preceding plots of peak-to-peak amplitude ratios for the Y displacement.

In order to better understand the dynamics of a strumming cable, each term in the above equation will be evaluated using the results obtained in this series of experiments. The following information is known for equation (4) and is based upon data from run #8.

Cable diameter	- 1.75 inches	k = 30.0 lbs/ft
Wetted length of cable	- 19.5 inches	mass = m = 7.87 lbs/32.2 ft/sec^2 m = 0.244 slugs
Cable weight	- 4.84 lbs/ft	f_s = 0.165 $\dot{X}$/D = 1.13 X, sec^{-1}

The remaining terms in equation (4) can be evaluated by examining the experimental results and Figure 3 which is a tracing of a "pluck test". Figure 3 was obtained by displacing the cable in the Y direction and releasing it. The resulting damped displacement vs time plot can be used to evaluate some of the remaining terms of equation (4).

The relation between the damped natural frequency q and the

undamped natural frequency ω_n is

$$q = \omega_n (1 - r^2)^{\frac{1}{2}} \tag{5}$$

and $r = C_3 / 2m\omega_n$, where r is the damping ratio (6)

and $\omega_n = \sqrt{k/m}$ (7)

Using the known values of k and m, equation (5) gives

$$\omega_n = \sqrt{30.0/0.244} = 11.09, \text{ rad./sec} \tag{8}$$

From Figure 3, the value of q can be determined.

$$q = 5 \text{ cycles} / 3.08 \text{ seconds} = 1.62 \text{ cps} = 10.2 \text{ rad./sec} \tag{9}$$

Using equation (5) to calculate the damping ratio

$$10.20 = 11.09 (1 - r^2)^{\frac{1}{2}}, \; r = 0.392 \tag{10}$$

Note that the potential for error in calculating the value of r is great; a small error in q or ω_n causes a disproportionate error in the results.

Using equation (6) to calculate the equivalent viscous damping coefficient C_3

$$0.392 = C_3 / 2(0.244)\, 11.09, \; C_3 = 2.12, \text{ lb-sec/ft} \tag{11}$$

The remaining unknown parameter is L, the equivalent forcing term in equation (4). It is convenient to define the magnification ratio M as

$$M = \frac{YK}{L} = \frac{1}{\left[(1-(\frac{\omega}{\omega_n})^2)^2 + (2\frac{\omega}{\omega_n} r)^2 \right]^{\frac{1}{2}}} \tag{12}$$

and use a value of Y = 1.35 inches corresponding to damped resonance, $f_{ny}/f_s \cong 1.0$, in Table I. Using $\omega = q$ in equation (12) will maximize

M.

$$M=\frac{1.35\ (30.0)}{(12.0)\ L} = \frac{1.0}{\left[(1-(\frac{10.2}{11.09})^2)^2 + (2x\frac{10.2}{11.09} \times 0.392)^2\right]^{\frac{1}{2}}} = 1.36 \qquad (13)$$

With M = 1.36, L becomes 2.49 pounds. Now equation (4) can be rewritten using the values of the parameters determined in the preceding equations to give

$$0.244\ \ddot{Y} + 2.12\ \dot{Y} + 30.0\ Y = 2.49\ \sin(2\pi f_s t) \qquad (14)$$

Using the same methods, the equations listed below were obtained for runs 5, 20-5.4, 20-10.5, and 20-20.5 respectively.

$$0.120\ \ddot{Y} + 1.71\ \dot{Y} + 30.0\ Y = 3.00\sin(2\pi f_s t) \qquad (15)$$

$$0.119\ \ddot{Y} + 1.48\ \dot{Y} + 16.8\ Y = 0.899\sin(2\pi f_s t) \qquad (16)$$

$$0.119\ \ddot{Y} + 1.48\ \dot{Y} + 16.8\ Y = 0.680\sin(2\pi f_s t) \qquad (17)$$

$$0.119\ \ddot{Y} + 1.48\ \dot{Y} + 16.8\ Y = 0.573\sin(2\pi f_s t) \qquad (18)$$

The reader is cautioned to use the utmost care in applying the preceding equations and data to prototype cases. This is particularly true when modeling a long cable with multiple short non-flexible hinged elements. In this case, the overall lateral spring rate relates to all model elements as a whole, rather than to each individual model element by itself. Said in another way, the lateral spring constant k used here is not the same as the lateral spring constant for an entire cable being modeled by a series of rigid hinged elements. The data presented here on mass and damping per unit length of cable are, however, directly applicable to such models.

CONCLUSIONS

1. The transverse oscillations of a strumming cable are closely predicted by simple second order linear theory when the Strouhal exciting frequency (f_s) is in the neighborhood of the cable's natural frequency (f_{ny}). A simple linear second order mathematical model could be used to make a rough estimate of the system response.

2. Hydrodynamic drag forces near the resonant point can be more than seven times the drag on a similar rigidly constrained cable. More experiments are needed to enable accurate prediction of the hydrodynamic drag on strumming cables since these results reflect only the results of several sets of experimental parameters (i.e., spring constants, mass of cable, amplitude of harmonic drive, etc.). Much could be learned by performing a similar series of experiments around a cable driven at constant velocity. This would have more application to mooring systems exposed to constant and slowly varying currents than the harmonically driven system used here.

3. The excitation frequency is closely approximated by the Strouhal vortex shedding frequency (Strouhal excitation frequency) in the range where the system natural frequency is greater than the Strouhal frequency. After the Strouhal frequency meets or exceeds the natural frequency of the system, the Strouhal frequency is no longer a good approximation to the exciting frequency.

4. In any system where an elastically constrained cylindrical or bluff

body is subjected to steady or unsteady transverse viscous flow, very significant flow induced resonant oscillations could readily lead to structural failure due to excessive strain, excessive stress or prolonged cyclic stress.

5. A thorough collection and examination of all available similar experimental results put into dimensionless format and plotted on single graphs would be a logical next step in drawing meaningful generalized conclusions about the phenomena described here. This would also be of great help in directing additional research to fill gaps and explain contradictions and inconsistencies in the data thus far produced. The experimental results described here can only be expected to contribute a small portion of the information leading to the formulation of generalized theories and explanations covering the entire useful range of parametric variations. Once this has been done, then it seems most logical to proceed on to the more complex and realistic problems associated with such things as continuously varying natural frequencies (a function of cable tension), the effect of previously shed vortices in the path of the oscillating cable, cable life predictions based upon the spectrum of cyclic stress in a sea water environment, and optimization of mooring designs with respect to cost, life expectancy, and reliability.

BIBLIOGRAPHY

1. Albertson, M. L., Barton, J. R. and Simons, D. B., Fluid Mechanics for Engineers, Prentice Hall, 61, pp 401.

2. Bidde, Devidas D., 1970 Wave Forces on a Circular Pile Due to Eddy Shedding, University of Calif., Hydraulic Engineering Laboratory, Report HEL 9-16, June 1970.

3. Casarella, M. J. and Parsons, M. A., Survey of Investigations on the Configuration and Motion of Cable Systems under Hydrodynamic Loading, Catholic University of America, Dept. of Mechanical Engineering, July-August 1970.

4. Dale, J. R., McCandles, J. M., and Holler, R. A., Water Drag Effects of Flow Induced Cable Vibrations, ASME Publication 68-WA/FE-47, 1968.

5. Fung, Y. C., Fluctuating Lift and Drag Acting on a Cylinder in a Flow at Supercritical Reynolds Numbers, Journal of the Aerospace Sciences, Vol. 27, Nov. 1960, pp 801-814.

6. Havelock, T. H., The Resistance of a Submerged Cylinder in Accelerated Motion, Quart. Journal of Mechanics and Applied Mathematics, Vo. II, Pt. 4, 1949.

7. Keim, R. S., Fluid Resistance to Cylinders in Accelerated Motion, Journal of the Hydraulics Division, ASCE, Vol 82, Paper 1113, December 1956.

8. Keulegan, G. H. and Carpenter, L. H., Forces on Cylinders and Plates in an Oscillating Fluid, Journal of Research of the National Bureau of Standards, Vol. 60, No. 5, May 1958, pp 423-440.

9. Laird, A. D. K., Johnson, C. H., and Walker, R. W., Water Eddy Forces on Oscillating Cylinders, Journal of the Hydraulics Division, ASCE, November 1960.

10. Laird, A. D. K., Water Forces on Flexible Oscillating Cylinders, Journal of Waterways and Harbors Division, ASCE, August 1962.

11. Marks, L. S., Mechanical Engineers Handbook, McGraw Hill, 58, 6th Edition, pp 8-213, 221.

12. Penzien, J., Wind Induced Vibration of Cylindrical Structures, Journal of the Engineering Mechanics Division, ASCE, January 1957.

13. Sarpkaya, T., Lift, Drag and Added Mass Coefficients for a Circular Cylinder Immersed in Time Dependent Flow, Journal of Applied Mechanics, Vol. 30, Series E, No. 1, March 1963, pp 16-24.

14. Weigel, R. L., Oceanographical Engineering, Englewood Cliffs, New Jersey, Prentice Hall, 1964, p 532.

LIST OF NOMENCLATURE

A' = Projected area of cable, $A' = \ell D$, ft^2

A = Crank arm radius for harmonic driver, inches

C_1 = Velocity squared damping coefficient, lbs sec^2/ft^2

C_2 = Empirical forcing function coefficient, dimensionless

C_3 = Equivalent viscous damping coefficient, lb sec/ft

C_d = Drag coefficient

D = Cable diameter, inches & feet

f_c = First mode natural frequency of one dimensional wave equation, cps

f_d = Main carriage driven frequency in the X direction, cps

f_y = Actual transverse (y direction) oscillation frequency and the true "excitation frequency", cps

F - Drag force for a rigidly constrained cylinder, $F = \frac{1}{2} C_d \rho AV^2$, lbs

f_{ny} = Damped natural frequency of oscillations in the Y direction, $f_{ny} = q$, cps

f_s = Strouhal vortex shedding frequency, cps

f_x = Actual oscillation frequency of F_{xmax} and F_{xmin} in the direction of flow, cps

F_{xmax} = Maximum average drag force in the X direction, lbs

F_{xmin} = Minimum average drag force near F_{xmax}, see Figure 13 for explanation, lbs

g = Acceleration of gravity, ft/sec^2

k = Linear spring constant, lbs/ft/19.5 inch cable model length

ℓ = Length of cable, ft

L = Equivalent forcing load, lbs

m = Mass of cable element plus mass of cross-carriage and transducers, $\frac{lb\ sec^2}{ft}$

m' = Virtual or added mass due to entrained water in the boundary layer, $\frac{\text{lb sec}^2}{\text{ft}}$

q = Damped natural frequency, $q = \omega_n(1-r^2)^{\frac{1}{2}}$, rad/sec

R = Reynolds Number

r = Equivalent linear damping ratio

T = Tension in cable, lbs

V_{max} = Maximum velocity in X direction, maximum value of $\dot{X}$, ft/sec

W = Weight per foot of cable, lbs/ft

$\dot{X}$ = Harmonic velocity in the X direction, ft/sec

$\dot{X}_{max}$ = Maximum harmonic velocity in the X direction, ft/sec

X = Harmonic displacement in the X direction, ft

Y = Transverse displacement of cross-carriage, inches

Y_{max} = Average of peak transverse displacements in Y direction, inches

ν = Kinematic viscosity, ft^2/sec

ω_n = Undamped natural frequency, $\omega_n = (k/m)^{\frac{1}{2}}$, rad/sec